KARADENIZ TECHNICAL UNIVERSITY
THE GRADUATE SCHOOL OF APPLIED SCIENCES

GEOMATICS ENGINEERING DEPARTMENT

A STATISTICAL-BASED FUSION TECHNIQUE FOR REMOTE SENSING IMAGES

MASTER OF SCIENCE THESIS

Deniz YILDIRIM

JANUARY 2013
TRABZON

KARADENİZ TEKNİK ÜNİVERSİTESİ
FEN BİLİMLERİ ENSTİTÜSÜ

HARİTA MÜHENDİSLİĞİ ANABİLİM DALI

A STATISTICAL-BASED FUSION TECHNIQUE FOR REMOTE SENSING IMAGES

Deniz YILDIRIM

Karadeniz Teknik Üniversitesi Fen Bilimleri Enstitüsünce
"Harita Yüksek Mühendisi"
Unvanı Verilmesi İçin Kabul Edilen Tezdir.

Tezin Enstitüye Verildiği Tarih : 18.12.2012
Tezin Sözlü Savunma Tarihi : 07.01.2013

Tez Danışmanı : Doç. Dr. Oğuz GÜNGÖR

Trabzon 2013

Karadeniz Teknik Üniversitesi Fen Bilimleri Enstitüsü

Harita Mühendisliği Anabilim Dalında

Deniz YILDIRIM tarafından hazırlanan

A STATISTICAL-BASED FUSION TECHNIQUE FOR REMOTE SENSING IMAGES

başlıklı bu çalışma, Enstitü Yönetim Kurulunun 18 / 12 / 2012 gün ve 1486 sayılı kararıyla oluşturulan jüri tarafından yapılan sınavda

YÜKSEK LİSANS TEZİ

olarak kabul edilmiştir.

Jüri Üyeleri

Başkan : Prof. Dr. Ertan GÖKALP …...……

Üye : Doç. Dr. Oğuz GÜNGÖR …...……

Üye : Doç. Dr. Murat EKİNCİ ……...……

Prof. Dr. Sadettin KORKMAZ

Enstitü Müdürü

ACKNOWLEDGEMENTS

This thesis would not have been possible without the help of certain people. With immense gratitude, I acknowledge the support and help of my advisor Assoc. Prof. Dr. Oğuz GÜNGÖR.

Also, I would like to express my special gratitude to my colleagues, in particular Res. Ass. Cemre YILMAZ, for their constant support throughout the research process.

I offer my regards and blessings to all of those who supported me in any respect during the completion of the thesis.

Lastly, I would like to thank my family for their help, for those many sleepless nights they stood by my side, and for their constant moral support. It is to my family that this thesis is dedicated to.

Deniz YILDIRIM
Trabzon 2013

THESIS STATEMENT

I hereby declare that all information in this thesis titled as "A Statistical-Based Fusion Technique for Remote Sensing Images" has been completed under the responsibility of my supervisor Assoc. Prof. Dr. Oğuz GÜNGÖR and presented in accordance with academic rules and ethical conduct. I also declare that, as required by these rules and conduct, I have fully cited and referenced all material and results that are not original to this work 18.12.2012.

Deniz YILDIRIM

TABLE OF CONTENTS

Page

ACKNOWLEDGEMENT III
THESIS STATEMENT IV
TABLE OF CONTENTS V
ÖZET VII
SUMMARY VIII
LIST OF FIGURES IX
LIST OF TABLES XI
NOTATIONS XII
1. GENERAL INFORMATION 1
1.1. Introduction 1
1.2. Objective of the Study 2
1.3. Definitions and Remarks 3
1.3.1. Image Space 3
1.3.1.1. Resampling by Dilations, Upsamplings and Downsamplings 4
1.3.2. Resolution and Other Key Properties 6
1.3.2.1. Spatial Resolution versus GSD 7
1.3.2.2. Spectral Resolution 7
1.3.2.3. Radiometric Statistics and Resolution 8
1.3.2.4. Temporal Resolution 9
1.3.3. Image Comparison, Closeness 9
1.3.3.1. Seminorms and Semi-inner Products 10
1.3.4. Flexibility Functions 11
1.4. Image Fusion 13
1.4.1. Image Fusion Techniques 14
1.4.1.1. Component- Substitution Techniques, IHS, PCA 14
1.4.1.1.1. IHS Method 15
1.4.1.1.2. PCA Method 16
1.4.1.2. Wavelet Transform and Haar Wavelet Method 18
1.4.1.3. Modulation-Based Techniques, Brovey 20
1.5. Quantitative Fusion Quality Assessment Techniques 21
2. CASE STUDY, DATA AND METHODOLOGY 24

2.1. Study Data 24
2.2. Methodology 28
2.2.1. Spectral Component 30
2.2.1.1. Covariance Based Spectrally Well Fused Image 32
2.2.1.2. Least Squares Based Spectrally Well Fused Image 34
2.2.1.3. Modification for Spectral Enhancement 36
2.2.2. Spatial Component 38
2.2.3. Final Fusion 43
3. FINDINGS 46
3.1. A Comparison of Fusion Results with Downsampling First 46
3.2 Choice of Coefficients for the Spatial Enhancements 47
3.3. Spectral, Spatial and Radiometric Quality Assessment Data 50
3.3.1. IHS Method 51
3.3.2. PCA Method 55
3.3.3. Haar Wavelet Method 58
3.3.4. Brovey Method 61
3.3.5. Covariance Based Method 64
3.3.6. Least Squares Based Method 67
3.3.7 Changing Flexibility Function Parameters 70
4. DISCUSSION AND CONCLUSION 71
5. REFERENCES 73
ÖZGEÇMİŞ

Yüksek Lisans

ÖZET

UZAKTAN ALGILAMA GÖRÜNTÜLERİ İÇİN İSTATİSTİK TABANLI BİR KAYNAŞTIRMA YÖNTEMİ

Deniz YILDIRIM

Karadeniz Teknik Üniversitesi
Fen Bilimleri Enstitüsü
Harita Mühendisliği Bölümü
Danışman: Doç. Dr. Oğuz GÜNGÖR
2013, 77 Sayfa

Dünya etrafında yörüngesinde seyahat etmekte olan birçok uzaktan algılama uydusu vardır ve bu uydular uzaktan algılama uygulama alanlarında kullanılmak üzere sürekli görüntü sağlamaktadırlar. Bu uyduların birçoğu her bir anda, farklı karakteristik özelliklere sahip ikişer görüntü üretirler. Bu iki görüntüden bir tanesi, yüksek konumsal çözünürlüklü bir pankromatik görüntü ve diğeri de daha düşük konumsal çözünürlüklü bir multispektral görüntüdür. Bu iki görüntüyü kullanarak bunlardan daha iyi kalitede yeni bir görüntü elde etmek için görüntü kaynaştırma kullanılır. Kaynaştırılan görüntü uydudan elde edilen multispektral görüntüden daha iyi konumsal çözünürlüğe sahip bir multispektral görüntüdür. Birçok görüntü kaynaştırma yöntemi vardır. Pankromatik görüntünün konumsal detayları yeni görüntüye aktarılabiliniyorsa ve orijinal multispektral görüntünün spektral içeriği korunuyorsa bu görüntü kaynaştırma yöntemi başarılıdır. Fakat, bu konuda bir denge unsuru vardır. Spektral içeriği iyi koruyan kaynaştırma yöntemleri ile genelde konumsal detay transferi konusunda eksiklikler yaşanmaktadır. Bazı uzaktan algılama uygulamaları için, spektral çözünürlük önemli iken bazıları içinse konumsal çözünürlük önemlidir. Uzaktan algılama uygulamalarındaki farklı ihtiyaçlara yönelik esnek bir teknik arzu edilmektedir. Bu araştırma, WorldView-2 görüntülerini kullanarak, popüler diğer görüntü kaynaştırma yöntemleri (IHS, PCA, dalgacık, Brovey görüntü kaynaştırma teknikleri) ile kıyaslayarak yeni ve esnek bir görüntü kaynaştırma yöntemi sunmaktadır. Önce spektral ve konumsal olarak iyi kalitede ara görüntüler oluşturulur. Bu görüntüler daha sonra, bir esneklik bileşeni aracılığıyla kaynaştırılır. Bu esneklik bileşeni oluşturulurken lokal varyans ve belirli koşulları sağlayan fonksiyonlar kullanılmıştır.

Anahtar Sözcükler: Görüntü, Kaynaştırma, Spektral, Konumsal, WorldView-2

Master Thesis

SUMMARY

A STATISTICAL-BASED FUSION TECHNIQUE FOR REMOTE SENSING IMAGES

Deniz YILDIRIM

Karadeniz Technical University
Department of Geomatics Engineering
Supervisor: Assoc. Prof. Dr. Oğuz GÜNGÖR
2013, 77 Pages

There are many artificial satellites in orbit, constantly providing imagery to be used in a wide range of remote sensing applications. Many of them acquire two images with different characteristics at a given time. One of these two images is a panchromatic image with a high spatial resolution, and the other one is a multispectral image with a lower spatial resolution. Image fusion is used to create a new image with superior qualities than these two images. The fused image is a multispectral image with a better spatial resolution than the multispectral image acquired by the sensor on satellite. There are many image fusion techniques available. An image fusion technique is successful, if the spatial detail of the panchromatic image is transferred into the new image, and the spectral content of the original multispectral image is preserved. There is a trade-off; a fusion technique preserving spectral content well tends to be lacking in spatial detail transfer quality. For some remote sensing applications, the spectral resolution is important, whereas for some others the spatial resolution is important. A flexible technique is desirable to accommodate to different needs of remote sensing applications. This research proposes image fusion techniques with flexibility and compares them against the popular image techniques (IHS, PCA, wavelet, Brovey image fusion techniques) and against each other, using WorldView-2 imagery. First intermediary images are created that have either spectrally or spatially good qualities. These are then fused together in a flexible manner using functions satisfying particular conditions and the local variance. This algorithm also enhances existing techniques.

Key Words: Image, Fusion, Spectral, Spatial, WorldView-2

LIST OF FIGURES

Page

Figure 1.1. Fusion procedure 2
Figure 1.2. Image space demonstration 3
Figure 1.3. GSD and number of spectral bands for several satellites 4
Figure 1.4. Graphs of f_r flexibility functions for a) $r<1$, b) $0<r<1$, c) $r>1$, d) $0<r<1$ 13
Figure 1.5. IHS Fusion Process 15
Figure 1.6. PCA components of Lena image 17
Figure 1.7. Two level wavelet decomposition 20
Figure 1.8. Wavelet method flow chart 20
Figure 2.1. Trabzon province marked red on a map of Turkey 24
Figure 2.2. Trabzon province with its districts 24
Figure 2.3. Spectral radiance responses 25
Figure 2.4. Input image pairs 26
Figure 2.5. Flow chart of the methodology 28
Figure 2.6. Covariance based method image example (zoomed) 34
Figure 2.7. Least squares method image example (zoomed) 36
Figure 2.8. Spectral Enhancement 37
Figure 2.9. Four composite images each of three images in T 40
Figure 2.10. Binary edge images of the panchromatic image 3, and its part in the complement of T 41
Figure 2.11. Flexibility component and local variance versus Sobel image 45
Figure 3.1. Images corresponding to different spatial coefficient configurations 49
Figure 3.1. (continued) Images corresponding to different spatial coefficient configurations 50
Figure 3.2. IHS images 52
Figure 3.3. IHS images zoomed to the upper left quadrant 53
Figure 3.4. PCA images 55
Figure 3.5. PCA images zoomed to the upper left quadrant 56
Figure 3.6. Haar wavelet images 58
Figure 3.7. Haar wavelet images zoomed to the upper left quadrant 59
Figure 3.8. Brovey images 61
Figure 3.9. Brovey images zoomed to the upper left quadrant 62

Figure 3.10. Covariance based method images 64
Figure 3.11. Covariance based method images zoomed to the upper left quadrant..... 65
Figure 3.12. Least squares based method images 67
Figure 3.13. Least squares method images zoomed to the upper left quadrant 68

LIST OF TABLES

Page

Table 2.1. Multispectral bands and spectral ranges 25

Table 2.2. Correlation statistics for the first image pair 27

Table 2.3. Correlation statistics for the second image pair 27

Table 3.1. Normalized MSE values for the fusion of downsampled images, no spatial enhancement 46

Table 3.2. Normalized MSE values for the fusion of downsampled images, best spatial enhancement configuration results 47

Table 3.3. Spatial coefficient configuration fusion quality statistics 48

Table 3.4. Fusion metrics for the upsampled original multispectral image 1 51

Table 3.5. Radiometric statistics for the upsampled original multispectral image 1 . 51

Table 3.6. IHS. Correlation statistics 54

Table 3.7. IHS. Fusion quality results 54

Table 3.8. IHS. Further radiometric statistics 54

Table 3.9. PCA. Correlation statistics 57

Table 3.10. PCA. Fusion quality results 57

Table 3.11. PCA. Further radiometric statistics 57

Table 3.12. Haar wavelet. Correlation statistics 60

Table 3.13 Haar. Fusion quality results 60

Table 3.14. Haar. Further radiometric statistics 60

Table 3.15 Brovey. Correlation statistics 63

Table 3.16. Brovey. Fusion quality results 63

Table 3.17. Brovey. Further radiometric statistics 63

Table 3.18. Covariance based method. Correlation statistics 66

Table 3.19. Covariance based method. Fusion quality results 66

Table 3.20. Covariance based method. Further radiometric statistics 66

Table 3.21. Least squares based method. Correlation statistics 69

Table 3.22. Least squares based method. Fusion quality results 69

Table 3.23. Least squares based method. Further radiometric statistics 69

Table 3.24. Flexibility function and parameter change. Fusion quality results 70

NOTATIONS

B1, B2,…., B8	Band1, Band2,…,Band8
ERGAS	Relative dimensionless global error in synthesis
GSD	Ground sample distance
IHS	Intensity, hue, saturation
IR	Infrared
IUPAC	International Union of Pure and Applied Chemistry
IWSSIM	Information content weighted version of SSIM
M	Mean radiance
M_k	Mean radiance of k^{th} spectral band
MSE	Mean squared error
NIR	Near infrared
P	Panchromatic
PCA	Principal components analysis
p_i	Pixel intensity values
RASE	Relative average spectral error
RMSE	Root mean squared error
SID	Spectral information divergence
SSIM	Structural similarity index
h/l	Ratio of resolution
μ	Mean
σ	Standard deviation
$\|\|\ \|\|$	Seminorm
$< , >$	Semi-inner product

1. GENERAL INFORMATION

1.1. Introduction

Remote sensing is the field of study associated with the acquisition of information about objects from a distance and without any physical contact. Objects affect their surrounding fields, and remote sensors, such as gravitometers, magnetometers, audiometers, and electromagnetic sensors (Lancaster, 1968), detect and measure the changes on the surrounding fields (Elachi and Van Zyl, 2006). This broad definition encompasses most of medical imaging, sonar and seismic imaging, vision, astronomy, and many other areas (Schott, 2007). In practice, the term remote sensing is restricted to the study of the digital imagery acquired by the electromagnetic sensors on the Earth-orbiting satellites (Konecny, 2003; Rees, 2001).

Remote sensing has a wide range of military and civilian applications (Rees, 2001). Especially in the last decade (Chen, 2012), many remote sensing systems have been developed for military surveillance and reconnaissance and applications in mapping, agriculture, environmental studies, meteorology (Schowengerdt, 2006), and disaster management (Nayak and Zlatanova, 2008). For the same scene, imagery from different sensors can easily be found, and these sensors provide complementary information (Chen, 2012). Remote sensing data from each sensor reflects only a portion of data, causing deficiency in information (Zhao, et al., 2002). A key concept in remote sensing is image fusion (Zhang, 2002).

Many modern remote sensing satellites provide at least two images for a scene at a given time, a multispectral image, and a panchromatic image. In image fusion, the images for the same scene are used together to obtain a superior image using the image fusion techniques (Gungor, 2008). On the panchromatic image, usually, geometric details can be better discerned, so the panchromatic image is spatially better than the multispectral image; the panchromatic image has a better spatial resolution. On the multispectral image, more colors can be discerned from each other than on the panchromatic image, so the multispectral image is spectrally better than the panchromatic image; the multispectral image has a better spectral resolution. The fused image is another multispectral image. Fused image is spatially better than the original multispectral image, but has similar

spectral content (Yang, et al., 2012). Fused image is more suitable for visual perception and computer processing and analysis (Mahyari and Yazdi, 2011). It has a meliorated visual effect (Wang and Liu, 2008). Fusion procedure is depicted in Figure 1.1.

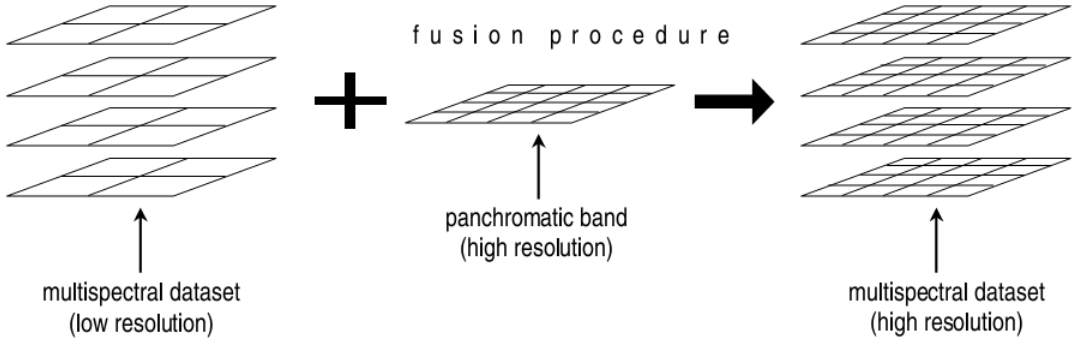

Figure 1.1. Fusion procedure (Hill, et al., 1999).

The wide range of applications of remote sensing does not have uniform needs. Applications in meteorology do not require high level of spatial resolution, whereas military surveillance applications require high level of spatial resolution (Schowengerdt, 2006). Similarly some applications, for instance in agriculture and forestry, require better spectral resolutions. The fusion techniques should have some flexibility and adapt to the users' needs and expectations.

Improving the spatial accuracy often degrades spectral quality. To meet the users' needs, on one hand, the techniques should be able to provide high spatial resolution fused images and also high spectral resolution ones, on the other hand, provide imagery in various spatial or spectral resolution levels.

1.2. Objectives of the Study

The primary objective of the study is to develop flexible and competitive image fusion techniques that produce spectrally and spatially good results, when compared to popular image fusion techniques. The secondary objective is to develop the theory in a manner open to improvements, allowing researchers to develop the settings for the applications (military or civilian) even further.

1.3. Definitions and Remarks

1.3.1. Image Space

Similar to matrix spaces, image spaces in remote sensing are real valued, topological vector spaces that can be embedded in sufficiently large Euclidean spaces (Pratt, 2001). Being vector spaces, addition and scalar multiplication are well defined as demonstrated in Figure 1.2. Algebraically viewed, with entry-wise multiplication, some image spaces can attain commutative ring structure (unlike matrix spaces). They have finite dimensions. One often works with compact subspaces (in particular with finite subsets) of image spaces that have a minimal attainable value (often 0) and a maximal attainable value (often 2^n -1, for some positive integer n). Each image then represents a land area on Earth. Physical quantities, such as radiance, are represented by the image entries, which are some quantized digital numbers (Liang, 2004).

Figure 1.2. Image space demonstration (3*red+2*green = orangish yellow)

For image fusion purposes, the image space for the original multispectral image should also contain the images whose bands are multiples of the panchromatic image. This will hold true, if the image space is the whole space of images with a given size. This way, the input image depending setting will be avoided, as well.

The images in an image space can have more than one band. Along other key properties, the size, given by the number of rows, columns, and bands, is constant for images in the same image space.

On images in an image space, the ground sample distance (GSD) is uniform. GSD is the distance between points on the ground corresponding to adjacent pixel centers. Smaller GSD indicates better spatial capability.

Figure 1.3. shows the graphical relation between GSD and the number of spectral bands for some Earth-orbiting satellite sensors on a logarithmic scale (Schowengerdt, 2006). The ones to the left like Quickbird panchromatic sensor have better spatial sensing capabilities.

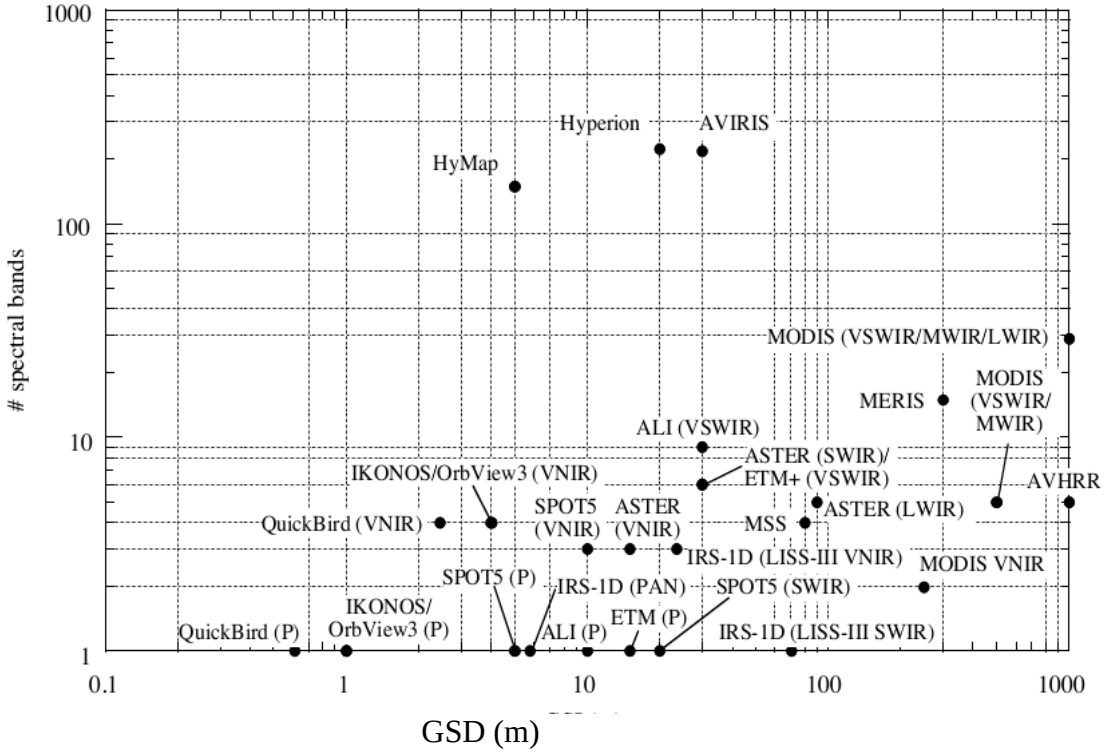

Figure 1.3. GSD and number of spectral bands for several satellites (Schowengerdt, 2006).

1.3.1.1. Resampling by Dilations, Upsamplings and Downsamplings

If two images have different GSD, where the ratio GSD_2/GSD_1 is a constant positive number k (often an integer), one can resample using the dilation function f(x,y)=(kx, ky) and make them have equal GSD. The pre-image of a pixel center under this dilation function is calculated, and one of the various resampling methods is applied. In general the

pre-image will not lie on the grid where the intensity values are defined. Various interpolation methods exist, assigning intensity values to points not on the grid.

The preferred method in the study is the nearest neighbor method, where the intensity values of nearest grid points to the pre-image become the intensity values of the resampled image. Other methods include the bilinear method, the cubic convolution and cubic spline interpolation (Goshtasby, 2005) (Mihov and Zapryanov, 2005). These methods are translation invariant. Nearest neighborhood method is fast, the intensity values on the resampled image are also intensity values of some of pixels on the original image. Intensity histograms before and after resampling are very similar (Goshtasby, 2005).

In bilinear resampling and cubic convolution resampling methods, the weighted average of the intensity values in a neighborhood of the pre-image point, is calculated and assigned as intensity value. The weights depend on the distance. In bilinear resampling, the neighborhood is the four nearest grid points horizontal and vertical distances to grid points (representing the pixel centers). First interpolate for the points on the horizontal gridlines using the grid points (x,y), as in (1). Then interpolate in the vertical direction using the points on grid lines and using (2).

$$I(x+\varepsilon, y)=(1-\varepsilon)\, I(x,y) + \varepsilon\, I(x+1,y), \text{ where } 0<\varepsilon<1 \text{ , } (x,y) \text{ grid point}, \quad (1)$$

$$I(x, y+\varepsilon)=(1-\varepsilon)\, I(x,y) + \varepsilon\, I(x,y+1), \; 0<\varepsilon<1, \; (x,y) \text{ on a horizontal grid line}. \quad (2)$$

This is extended to the second neighborhood for the cubic convolution resampling using (3) – (8) (Goshtasby, 2005).

$$I(x+\varepsilon, y) = \sum_{-1}^{2} fj(\varepsilon)\, I(x+j, y) \text{ , where } 0<\varepsilon<1 \text{ , } (x,y) \text{ grid point}, \quad (3)$$

$$I(x, y+\varepsilon) = \sum_{-1}^{2} f_j(\varepsilon)\, I(x, y+j) \text{ , } \; 0<\varepsilon<1 \text{ , } (x,y) \text{ on horizontal grid line}, \quad (4)$$

where the functions f_j are defined as follows.

$$f_{-1}(\varepsilon) = -3\frac{\varepsilon\,(1-\varepsilon)^2}{2} \quad (5)$$

$$f_0(\varepsilon) = \frac{(\varepsilon-1)(3\varepsilon^2-2\varepsilon-2)}{2} \quad (6)$$

$$f_1(\varepsilon) = -\frac{\varepsilon\,(3\varepsilon^2-4\varepsilon-1)}{2} \quad (7)$$

$$f_2(\varepsilon) = \frac{\varepsilon^2(\varepsilon-1)}{2} \quad (8)$$

For cubic spline resampling, the function f_j change to the ones in (9)-(12) (Goshtasby, 2005).

$$f_{-1}(\varepsilon) = \frac{(1-\varepsilon)^3}{6} \quad (9)$$

$$f_0(\varepsilon) = \frac{3\varepsilon^3-6\varepsilon^2+4}{6} \quad (10)$$

$$f_1(\varepsilon) = -\frac{\varepsilon\,(3\varepsilon^2-4\varepsilon-1)}{2} \quad (11)$$

$$f_2(\varepsilon) = -\frac{(3\varepsilon^2-3\varepsilon^2-3\varepsilon-1)}{6} \quad (12)$$

Resampling is called downsampling or upsampling, depending on the value of k. If $k>1$, it is a downsampling, and if $0<k<1$, it is an upsampling. Resampling enables relations between different image spaces that have different GSD.

Associated methods of upsampling and downsampling should be used in an application. If a function is integrated with respect to a variable, and then differentiated with respect to the same variable, one gets the original function. Analogously, for associated upsampling and downsampling methods, if an image is first upsampled and then downsampled, the original image should be obtained.

1.3.2. Resolution and Other Key Properties

For images, four different resolutions are defined. They are spatial resolution, spectral resolution, radiometric resolution, and temporal resolution

1.3.2.1. Spatial Resolution versus GSD

Spatial resolution of an image is the distance on ground between two parallel lines that can be resolved on the image. The maximal spatial resolution gives the minimal possible size of a square shaped region that can be distinguished on the image from its surroundings. On a satellite image with a spatial resolution of 1m, a square object 1m wide and 1m long can be distinguished; the distance between opposite sides is 1m, so they can be separated.

GSD gives a bound and generally a good estimate for the spatial resolution. An upsampled image would have a smaller, so better, GSD, but same set of objects on ground should be able to be resolved from the image, hence spatial resolution would not change significantly.

WorldView-2 panchromatic images have a GSD and spatial resolution of approximately 50cm (Madden, 2011).

1.3.2.2. Spectral Resolution

According to IUPAC's Green Book (1993), spectral resolution is the frequency or wavelength difference of two still distinguishable lines in the electromagnetic spectrum. IUPAC's definition is analogous to the usual definition of spatial resolution, the spatial domain being replaced by the spectral feature space. Spectral resolution gives the level at which different shades of similar colors (spectral frequency) can be resolved.

The spectral resolution is related to the number, width and spectral range of the bands. Typically, if the image has more bands and if the bandwidths are narrower, the spectral resolution is better. If the color is homogenous throughout the image, the spectral resolution is low for that particular image, even if the sensor had better spectral capabilities. In an image, repeating bands won't enhance the spectral resolution.

Hyperion sensor images have one of the best spectral resolutions, as it can be seen in Figure 1.3. They have over 200 bands, and the bandwidths are as narrow as approximately 10nm. 14 different shades of red can be distinguished using Hyperion sensor imagery (Yıldırım and Güngör, 2012). WorldView-2 images have 8 spectral bands (Padwick, et al., 2010) and one panchromatic band.

Most humans are trichromats and have three color vision (red, green, blue). Neitz, et al. (2001) estimates that 99 million women in the world can be tetrachromats, so have four color vision and see 100 million colors instead of 1 million.

1.3.2.3. Radiometric Statistics and Resolution

Radiometric statistics are related with the distribution of intensity values. They do not convey neighborhood or inter-band relation information. If the pixels are moved around the image, radiometric statistics do not change. Radiometric statistics uniform on images acquired by the same sensor includes the dynamic range.

Dynamic range is often given in logarithmic terms as in (13). For WorldView-2 multispectral and panchromatic sensor imagery, the maximal attainable pixel intensity value is 2047, and minimal attainable pixel intensity value is 0. Therefore they have a dynamic range of 11 bits (Padwick, et al., 2010).

$$Dynamic\ range \stackrel{\text{def}}{=} \log_2\left(\frac{maximal\ \ attainable\ \ value+1}{minimal\ \ attainable\ \ value+1}\right)\ bits \tag{13}$$

Other radiometric type statistics include entropy, minimal and maximal intensity values, contrast and diversity of images. Contrast, or "rms contrast", is the standard deviation of pixel intensity values (Peli, 1990).

Entropy is the Shannon entropy of information theory, as defined in (14), measuring unpredictability, disorder, and information content (Hamza, et al., 2005).

$$Entropy \stackrel{\text{def}}{=} -\sum p_i \log_2(p_i)\ , \tag{14}$$

where p_i are pixel intensity values.

Diversity is the number of distinct pixel intensity values in the image. If defined logarithmically as in (15), and will be smaller than the dynamic range.

$$Diversity \stackrel{\text{def}}{=} \log_2(number\ of\ distinct\ intensity\ values)\ bits \tag{15}$$

Diversity is a closer indicator to radiometric resolution than the dynamic range. Radiometric resolution indicates the level of the identified difference in close values of intensity, and of how finely the intensity values are represented (URL-1, 2012; URL-2, 2012).

Further radiometric statistics include some threshold values. Cornet, et al. (2001) chose three percent thresholds th_3 and th_97. Three percent of all pixel intensity values lie below th_3, and three percent of them lie above th_97. In this study, 2.275 percent thresholds are chosen. If the data were normally distributed with mean μ and standard deviation σ, this would correspond to 2σ thresholds; approximately 2.275% of data would lie below $\mu-2\sigma$ and 2.275% of data would lie above $\mu+2\sigma$.

1.3.2.4. Temporal Resolution

A basic indicator for the temporal resolution indicating how frequently images are acquired for the same scene is the revisit rate of the satellite (URL-1, 2012). Different satellites travel at different frequencies around the Earth. WorldView-2 revisit rate is 3.7 days for the maximal spatial resolution of approximately 50cm (URL-3, 2012). Due to overlaps in image swath (whose coverage depends on the latitudes), images are taken for the same scene more frequently than the revisit rate, but with lower spatial resolution (URL-1, 2012). WorldView-2 panchromatic sensors acquire images for the same scene with a spatial resolution of 1m or better every 1.1 days (URL-3, 2012).

1.3.3. Image Comparison, Closeness

For images in the same image space, a natural question arises about how to compare them. The standard tool is the mean squared error (MSE) (Wang, et al., 2004). One takes the difference of the images, and squares it entry-wise. As can be inferred from its name, MSE is then the mean value of the squared difference image. Root mean squared error (RMSE) is the square root of MSE. RMSE is related with the Frobenius norm of the error image regarded as a matrix.

Norms are positive homogenous real valued functions, for which the triangle inequality holds true, and the zero element is the only element whose norm is 0. For every

other element, the norm is strictly positive. Norms generalize absolute values of complex numbers and lengths of vectors, and they can further be generalized to seminorms. Seminorms can have non-trivial kernel spaces.

1.3.3.1. Seminorms and Semi-inner Products

A seminorm || || on an image space satisfies the following three properties (URL-4, 2005):

- $|| \lambda A || = |\lambda| \, ||A||$ for any real number λ and any image A (homogeneity)
- For any two image A and B, $|| A + B || \leq ||A|| + ||B||$ (triangle inequality)
- $||A|| \geq 0$ for any image A (non-negativity)

Seminorms give a measure of closeness. A is closer to B than C is to B, if $||A-B|| \leq ||C-B||$ (URL-4, 2005). As opposed to norms, seminorms can have nonzero kernels, seminorm of a nonzero element may equal to 0.

From triangle inequality, it follows that for any seminorm, $||A+B||^2 + ||A-B||^2 \leq 2 \, ||A||^2 + 2 \, ||B||^2$.

Some seminorms satisfy the parallelogram identity in (16).

$$||A+B||^2 + ||A-B||^2 = 2 \, ||A||^2 + 2 \, ||B||^2 \quad \textit{for A and B in the image space} \qquad (16)$$

Semi-inner products can be associated with seminorms that satisfy parallelogram identity. Let λ be a real number, and let A, B and C be images. A real valued semi-inner product <, > satisfies the following (URL-5, 2012):

- $< \lambda A + B, C > = \lambda <A,C> + <B,C>$ (linearity in the first component)
- $<A, B> = <B, A>$ (symmetry)
- $<A,A> \geq 0$ (positive semi definite)

For complex valued semi inner products, conjugate symmetry applies instead of symmetry (URL-5, 2012). Linearity in the second component follows from the first two conditions.

Given a semi-inner product <,>, there is a seminorm || || associated with it. For any image A, $||A||^2 = <A, A>$ (URL-5, 2012).

This induced seminorm satisfies the parallelogram identity.

$||A+B||^2 + ||A-B||^2 = <A+B,A+B> + <A-B,A-B> = <A,A>+<A,B>+<B,A> + <B,B>$
$+ <A,A>-<B,A>-<A,B>+<B,B> = 2<A,A>+2<B,B> = 2\,||A||^2 + 2\,||B||^2$

Notice that for real numbers a and b, $ab = ((a+b)^2 - (a-b)^2)/4$. In the past, this relation was used for multiplications of large numbers with tables listing square values.

If a real valued seminorm || || satisfies the parallelogram identity, the construction in (17) yields a semi-inner product.

$\langle A, B\rangle = \frac{\|A+B\|^2 - \|A-B\|^2}{4}$ for images A, B in the image space. (17)

Furthermore, the seminorm induced by this semi-inner product is the original seminorm || ||. $\langle A, A\rangle = \frac{\|2A\|^2 - \|0\|^2}{4} = \|A\|^2 \geq 0$.

For such pairs of seminorms and semi-inner products, Cauchy-Schwarz inequality in (18) holds for image spaces with associated semi-inner products and seminorms (URL-5, 2012).

$| < A, B > | \leq ||A||\,||B||$ for any images A, B in the image space. (18)

For images A and B in an image space with a semi-inner product <, >, the angle between A and B is the number α in [0, π] be such that <A, B> = ||A|| ||B|| cos(α). α exists as a real number by Cauchy-Schwarz inequality.

Under (Cauchy sequence) completeness, Hausdorff image spaces become Fréchet spaces (Bierstedt and Bonet, 2003).

Multiplication of real numbers and in real modular arithmetic and dot products for vectors are some basic examples of semi-inner products. Another example is covariance of images.

1.3.4. Flexibility Functions

The flexibility functions map the unit interval to itself smoothly with non-smooth limits. They will be used to create the flexibility component in fusion with the local variances.

A series of functions will be called flexibility functions if they satisfy the following properties.

1. f_r are continuous on [0,1], f_r' exist and are continuous on (0,1).
2. f_r' are nonnegative on (0,1).
3. f_r are convex for $r \geq 1$ and concave for $0<r\leq 1$
4. $f_r(0)=0$, $f_r(1)=1$
5. As r approaches s in (0,1), f_r approaches f_s in $L\infty([0,1])$
6. As r decreases to 0, f_r approaches to g in $L\infty([0,1])$, where g(x)=1 for x in (0,1], g(0)=0
7. For every $\varepsilon>0$, there exists R_ε, such that for all $r>R_\varepsilon$, $\|f_r-h\|\infty<\varepsilon$, where h(x)=0 for x in [0,1), h(1)=1 (Yıldırım and Güngör, 2012).

The first two conditions are the smoothness conditions. Being continuous on the unit interval, these functions attain their minimum and maximum values. They are smooth on the open interval (0,1), but the derivative may for instance diverge to infinity at the end points. The functions are non-decreasing, preserving order. Due to concavity/convexity, relevant Jensen's inequalities apply (Kuczma, 2008).

Two examples are listed in (19) and (20). Convex combinations of flexibility function series are also flexibility function series. Other flexibility function series exist, some of them involve hypergeometric functions, as defined in Dutka (1984).

$$f_r(x) = r^{\frac{1-r^{-x}}{r-1}} \tag{19}$$

$$f_r(x) = x^r \tag{20}$$

If r=1/4, function in (19) becomes $(4^x-1)/3$, and function in (20) becomes $\sqrt[4]{x}$. In Figure 1.4., the various flexibility functions are plotted for different r values. For r=1, the flexibility function equals to the identity function f(x)=x. For r>1, the flexibility functions are convex, and as r increases to infinity, the functions decrease to the downwards integer rounding function (floor). For positive r<1, the functions are concave, and approach the upwards integer rounding function (ceiling) as r approaches 0. For function series in (19) and (20), they approach monotonously. The function series in (20) approaches more quickly to the limits.

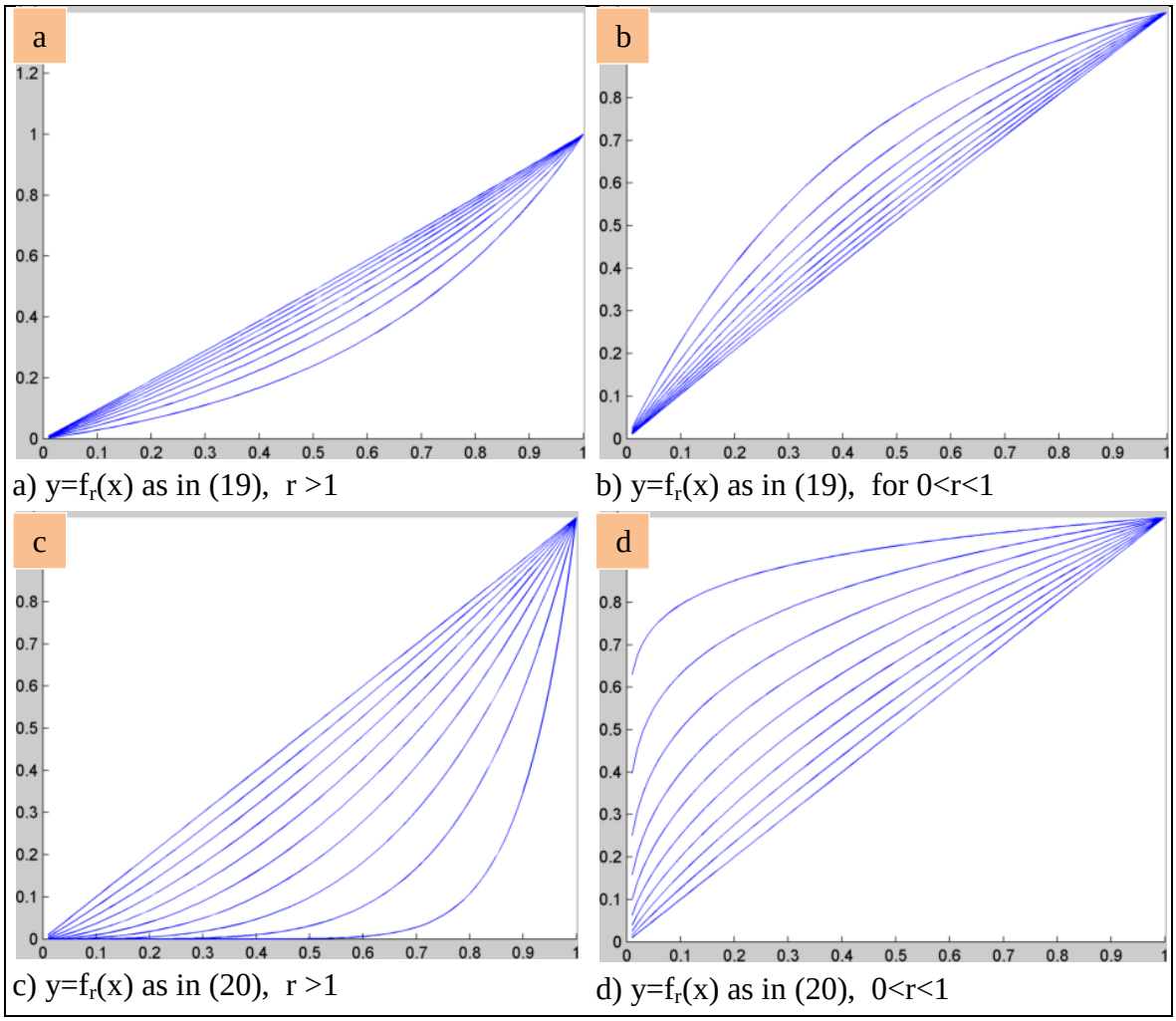

a) $y=f_r(x)$ as in (19), r >1

b) $y=f_r(x)$ as in (19), for 0<r<1

c) $y=f_r(x)$ as in (20), r >1

d) $y=f_r(x)$ as in (20), 0<r<1

Figure 1.4. Graphs of f_r flexibility functions for a) r<1, b) 0<r<1, c) r>1, d) 0<r<1

1.4. Image Fusion

Many modern remote sensing satellites regularly produce both panchromatic and multispectral imagery for the same place at a given time. The panchromatic image typically has a larger spectral range; hence the panchromatic detector cells can be built smaller for the same energy level. This increases the number of cells for the same area. For this reason and for data storage reasons, on a satellite that provides simultaneous panchromatic and multispectral imagery, the panchromatic image has smaller GSD and better spatial resolution (Zhang, 2004). With image fusion, one overcomes this problem to some extent.

Image fusion is meaningful, if the images are co-registered and represent the same area. The images may have different spatial/spectral/radiometric/temporal resolutions. The

fused images have better spatial resolution than the original multispectral images. The spatial resolution should be close to the spatial resolution of the original panchromatic image (Pohl and Van Genderen, 1998). At the same time, the spectral content is to be preserved well (Cliche, et al., 1985). Radiometric resolution should not be downgraded.

As an example, for IKONOS imagery with 1m panchromatic spatial resolution and 4m multispectral spatial resolution, the fused image can reach a spatial resolution of 1.3m (Švab and Oštir, 2006).

Especially for input images from different sensors, a helpful operation before fusion is histogram matching as described in (Gonzalez and Woods, 2008).

1.4.1. Image Fusion Techniques

According to Zhang (2008), image fusion techniques can be divided into three categories. These are the category of component substitution techniques (e.g. IHS and PCA), the category of multi-scale analysis-based fusion techniques and the category of modulation-based techniques (e.g. Brovey method). The multi-scale analysis-based techniques use wavelet decomposition (Zhang, 2008). Combinations of these methods exist (Chibani and Houacine, 2002).

1.4.1.1. Component Substitution Techniques, IHS, PCA

The component substitution techniques proceed in three steps and involve forward and backward transformations between the image space and another image space. First, a forward transform is applied to the multispectral bands to get the representation and components in the new space. In this new space, a particular component is chosen. This component should theoretically and in practice be the component that most resembles the panchromatic image. This particular component is replaced by the panchromatic image. Lastly, the inverse transform is applied (Jinghui, et al.). IHS and PCA methods are the most known representatives of the component substitution methods.

1.4.1.1.1. IHS Method

In IHS color space, I is the intensity component, H stands for hue, which gives the dominant color as an angle, and S stands for saturation. It is a conical representation of the rectangular RGB space. An orthonormal transformation is shown in (21).

$$\begin{bmatrix} I \\ S\cos(H) \\ S\sin(H) \end{bmatrix} = \begin{bmatrix} \frac{1}{\sqrt{3}} & \frac{1}{\sqrt{3}} & \frac{1}{\sqrt{3}} \\ \frac{1}{\sqrt{6}} & \frac{1}{\sqrt{6}} & \frac{-2}{\sqrt{6}} \\ \frac{1}{\sqrt{2}} & \frac{-1}{\sqrt{2}} & 0 \end{bmatrix} \begin{bmatrix} R \\ G \\ B \end{bmatrix} \tag{21}$$

Intensity component of a multispectral image contains its spatial component (Chibani and Houacine, 2002), whereas hue and saturation components retain the spectral information (González-Audícana, et al., 2006; Gonzalez-Audicana, et al., 2005; Pohl and Van Genderen, 1998). As in many other pixel level fusion techniques, the original multispectral image is upsampled, and this upsampling, which has the same GSD with the panchromatic image, is fused with the panchromatic image. Each upsampled band is transformed, and the resulting intensity component is replaced by the panchromatic image while hue and saturation parameters are kept unchanged. IHS transformation is well-defined for three bands, but it can be generalized to higher dimensions, still with orthonormal transformations (Gungor, 2008). Also, one may choose to fuse all bands, or some of them, for instance three of them. A flow chart of IHS fusion process is shown in Figure 1.5.

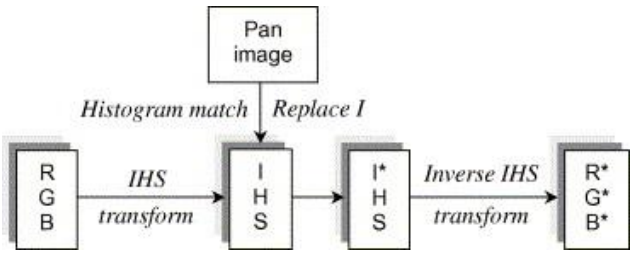

Figure 1.5. IHS Fusion Process (Zhang and Hong, 2005).

IHS transformation is a basic, linear transformation. The invertible transformation matrix can be chosen in a variety of ways. The first row corresponds to the intensity

component. The row vectors should be orthogonal with each other (their dot product should be zero) (Harrison, et al., 1990). It will turn out that the choice of row entries, other than the first row, is not as important. The first row gives the weight in intensity calculations. If only three bands are fused, all but three corresponding entries in the first row are zero. The best weights depend on the imaging sensor, and they need to be calculated. Choi, et al. (2006) calculated the best linear approximation weights for IKONOS images, and found that *I= Red/10 + Green/4 + Blue/12 + 17 Near Infrared/30* is the best linear approximation. The first row entries of the preferred version in this study are all 1, so equal weights are assumed. Taking the spectral ranges of WorldView-2 bands into account, the first and last entries of the first row of the transformation could be set to 0.

It turns out that the whole process is just adding the same value (the difference between I and a fixed multiple of the panchromatic image intensity values) to each band, leading to faster execution of the IHS method. It also causes spectral distortion. IHS method performs well spatially, but not so well spectrally (Tu, et al., 2004). Due to its fast execution and spatial qualities, it is one of the most commonly used fusion techniques.

1.4.1.1.2. PCA Method

The second popular component substitution technique that will be discussed is the principal components analysis (PCA) method (Zhang, 2010). The PCA transforms the multispectral data into linearly independent components, its principal components, according to the covariance matrix of the multispectral image and its eigenvalues. The covariance matrix and the eigenvalues are calculated using the singular value decomposition.

The first principal component corresponds to the absolutely largest eigenvalue of the covariance matrix of the multispectral bands and the rest of the principal components are sorted likewise.

The first principal component contains the spatial detail information of the multispectral image, whereas the remaining principal components contain the spectral information content of the multispectral image (Chavez, 1989; González-Audícana, et al., 2004; Zhou, et al., 1998).

The first principal component is replaced with higher spatial resolution panchromatic image and the inverse PCA transform is applied to get the fused image (Gonzalez and

Woods, 2008). The performance of this statistical method depends greatly on the input images (Gungor, 2008). Being another component substitution method, the flow chart of PCA method resembles the flow chart of IHS method in Figure 1.5.

To demonstrate the effect of the PCA transform, the popular three color 8 bit Lena image and its PCA components are shown in Figure 1.6. The first PCA component contains most of spatial details of the image. The last component is hardly distinguishable from a solid black image. Maximal attainable value, mean radiance and standard deviation of the last component are 255, 0.1617, and 1.0121 respectively. The image needed a dynamic range of at least 11 bits to have a mean radiance over 1, to have a mean radiance that counts.

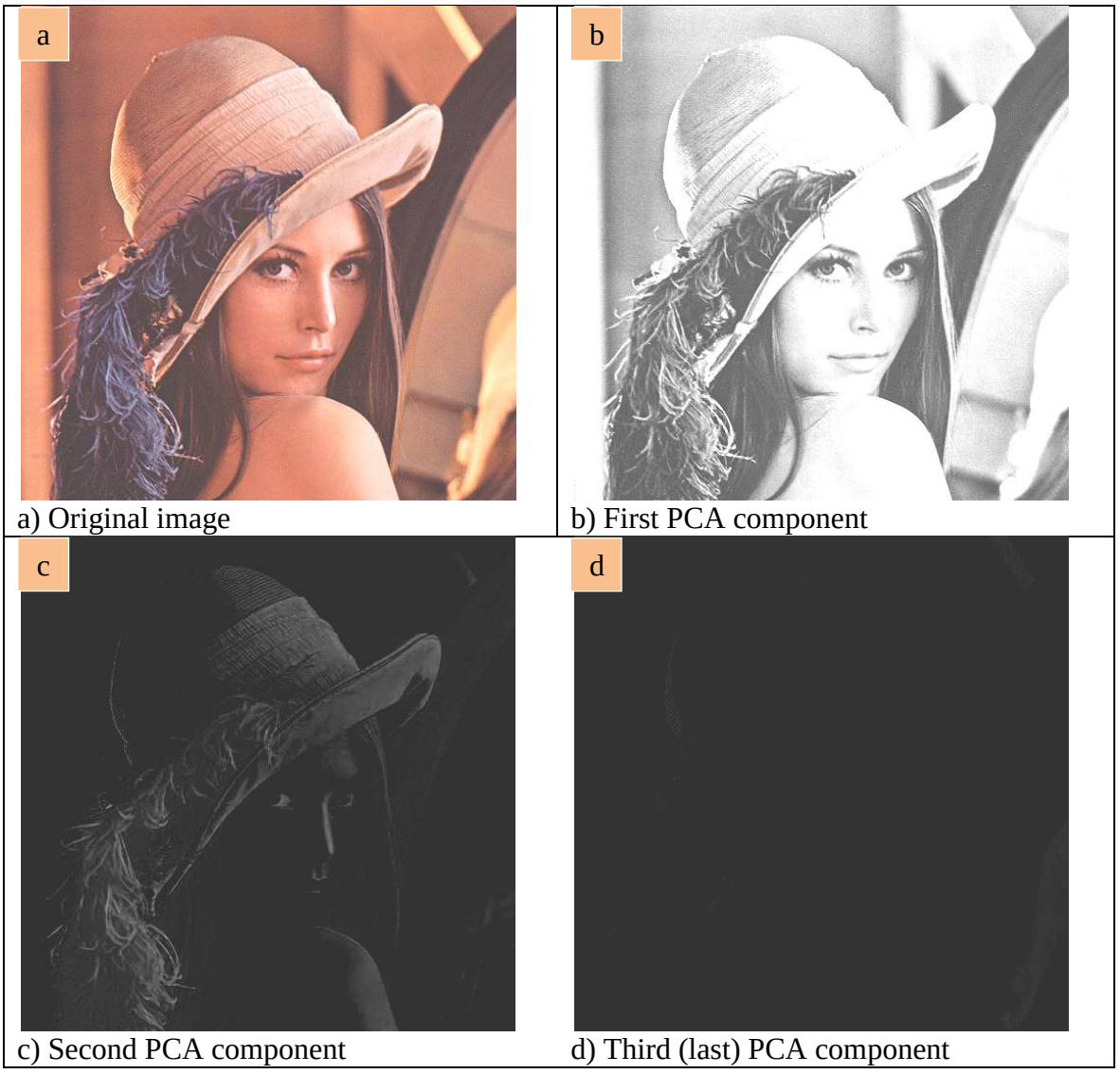

a) Original image

b) First PCA component

c) Second PCA component

d) Third (last) PCA component

Figure 1.6. PCA components of Lena image

PCA transform can also be used to reduce the number of bands, by removing the latter bands, and then applying the inverse PCA transform for the new number of bands. This also decreases storage needs.

1.4.1.2. Wavelet Transform and Haar Wavelet Method

Wavelet transform allows decomposing an image into both space and scale (Farge and Schneider, 2006). It is similar to Fourier transform, but instead of sine and cosine base functions, one has mother wavelet functions generating the wavelets. Furthermore, similarly, an orthogonal basis consisting of wavelets exists, generating square integrable functions on [0,1].

Continuous mother wavelets Ψ are functions that are both square integrable and absolutely integrable (so in L^2 and L^1 spaces on their domain), with an L^2 norm of 1, and have zero mean (Chui, 1992). So,

- $\int |\Psi|^2 \, dx = 1$
- $\int |\Psi| \quad dx < \infty$
- $\int \Psi \quad dx = 0$

Daughter wavelets $\psi_{a,b}$ are obtained by translation and scaling and then normalizing mother wavelet functions, as in (22).

$$\psi_{a,b}(x) = \sqrt{\frac{1}{a}} \quad \Psi\left(\frac{x-b}{a}\right) \tag{22}$$

In (18), a is the scaling factor, and b is the translation factor (Amolins, et al., 2007). Often a and b are chosen such that $j = -\log_2(a)$, and $k = b/a$ are integers. Then (22) can be rewritten as in (23).

$$\psi_{j,k}(x) = \sqrt{2^j} \quad \Psi(2^j x - k) \tag{23}$$

Changing the parameter j by 1 causes a dilation by 2 (Amolins, et al., 2007). The wavelet functions can be discretized.

Mother wavelets exist, one example is the Haar wavelet defined as in (24) and Haar wavelet is the mother wavelet used in this study.

$$\psi(x) = \begin{cases} 1 & \text{if } 0 \le x < 1/2, \\ -1 & \text{if } \frac{1}{2} \le x < 1, \\ 0 & \text{otherwise.} \end{cases} \tag{24}$$

By applying the wavelet transform once on an image, two lower resolution images are produced, the approximation image, and the high frequency component. Applying the wavelet transform once more on each of these two images results in 4 images, the level 2 wavelet components, the scale space representation of the original image in 4 times lower resolution. Using these wavelet components, and applying the corresponding inverse wavelet transforms, one gets the original high resolution image.

The wavelet methods start with decomposing the panchromatic image enough many times, and getting the scale space representation at the resolution of the multispectral image, the low resolution image.

If the ratio of resolutions is 4, the panchromatic image is decomposed twice, resulting in 4 images, the DD component (high frequency component of the level 1 high frequency component), the VD component (approximation image of the level 1 high frequency component), the HD component (high frequency component of the level 1 approximation image), the A component (approximation image of the approximation image) as in Figure 1.7.

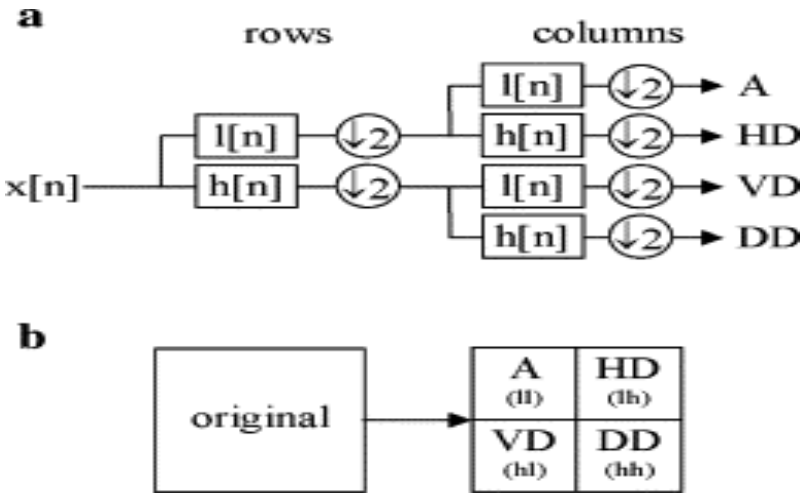

Figure 1.7. Two level wavelet decomposition (Amolins, et al., 2007).

The A component should resemble bands of multispectral image. The bands of multispectral image are compared with the A component. The high frequency components of the panchromatic image are added to the bands of the multispectral image, and inverse wavelet transformation is applied, as demonstrated in Figure 1.8. Wavelet method causes block shaped artifacts (Li, et al., 1995).

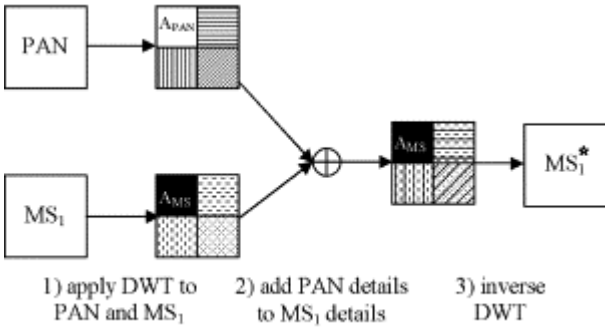

Figure 1.8. Wavelet method flow chart (Amolins, et al., 2007).

1.4.1.3. Modulation-Based Techniques, Brovey

In modulation-based techniques, first an intermediary image is created from the input images, and then the ratio of the panchromatic image and the synthetic image is multiplied by the upsampled multispectral image, band by band, to get the fused image (Jinghui, et al.). A popular modulation-based technique is Brovey method, where the synthetic image is the sum of the multispectral bands. First, each multispectral band is normalized,

dividing by the sum of all spectral bands (adding a small constant), and then they are multiplied by the panchromatic band (Zhang, 2002).

Brovey method was developed to produce visually appealing images from three band multispectral images and panchromatic images of urban areas by increasing the contrast in low (eg. shadows of buildings, trees) and high ends (Nikolakopoulos, 2008).

1.5. Quantitative Fusion Quality Assessment Techniques

Mean squared error analysis is a standard tool in quality assessment in signal theory. It is useful in image fusion, as well. Many image fusion quality assessment metrics have been proposed, none has become the one and only standard. They have all their quality points over other pre-existing metrics and MSE.

ERGAS (Relative dimensionless global error), SID (Spectral Information Divergence), SSIM (Structural Similarity Index) and IWSSIM (Information content weighted SSIM) are the chosen quality assessment metrics. They are used together with the band correlation change analysis to assess the spatial, spectral, and radiometric fusion quality.

In the settings where natural groupings exist, and in the case that these groupings occur in the same or in an analogous fashion for both sides of the comparison, statistics reflecting or using this grouping structure should be better than the statistics calculated using the whole bulk of data at one.

As multispectral images can have many bands, fairly independent from each other, MSE for the whole images at once may not give the desired results. Relative average spectral error (RASE) is an improvement taking the multispectrality into account (Wald, 2000). MSE is calculated for each band separately. The percentage ratio of the square root of the average MSE over bands over the mean radiance gives the RASE.

In image fusion, typically the multispectral image is upsampled. The GSD becomes the same with the GSD of the panchromatic image, but the resolution stays low. The resolution difference needs to be taken into account.

Relative dimensionless global error in synthesis (“Erreur elative globale adimensionnelle de synthese", ERGAS) is an improvement on RASE, taking the resolution difference into account (Wald, 2000). An ERGAS value smaller than three indicates a fusion preserving spectral content well (Aiazzi, et al., 2004). Optimal value is 0.

Formula for ERGAS is given in (25).

$$ERGAS = 100\frac{h}{l}\sqrt{\frac{1}{K}\sum_{k=1}^{K}\frac{MSE(k^{th}Band)}{M_k{}^2}} \quad (25)$$

where h/l is the ratio of resolutions (Wald, 2000) and M_k stands for the mean radiance of the k^{th} spectral band of a total of K spectral bands (Gungor, 2008).

Band correlation analysis is another tool in analyzing how much the spectral content is preserved. The similarity levels between the bands should change as small as possible after the fusion, as the fusion process is meant to preserve spectral content. CC, the correlation coefficient metric is the RMSE between the band correlations before and after the fusion. Small values indicate close spectral content (Rahmani, et al., 2010). Optimal value is 0.

In SID, the aim is to find a probabilistic relation scale for the pixel values of the compared images, when viewed as random variables (Chang, 1999). SID is the sum of relative entropies (Chang, 1999). Optimal value is 0. SID values closer to 0 indicate that probabilistically, the pixel values are more similarly distributed. It is a radiometric type metric.

Wang, et al. (2004) created the SSIM index, which is an improvement on their previous spatial index UIQI (Universal image quality index) that measures the structural similarity between images. It involves calculating the directional means and standard deviations for each window w of a particular size, swept through moving windows over entire images. The formula is shown in (26).

$$SSIM(x,y|w) = \frac{(2\bar{w}_x\bar{w}_y+C_1)(2\sigma_{w_xw_y}+C_2)}{(\bar{w}_x^2+\bar{w}_y^2+C_1)(\sigma_{w_x}^2\sigma_{w_y}^2+C_2)} \quad (26)$$

Averaging the SSIM values over windows, gives the SSIM value for the two monochromatic images. To calculate SSIM value for the fusion, a monochromatic image representing the multispectral image (for instance the mean over bands) is compared against the original panchromatic image.

IWSSIM is the information content weighted version of SSIM (Wang and Li, 2011). The SSIM values for windows are calculated, but now they don't have the same weights.

The weights are determined using a logarithmic function of the local variances (Wang and Shang, 2006). So, the regions where the local variances are high contribute more to the final IWSSIM value. For two fusion techniques that yield the same final SSIM value, if one does spatial detail transfer better around the edges, that one will yield a higher IWSSIM than the other one.

IWSSIM and SSIM are valued between 0 and 1, and the values closer to 1 indicate better spatial detail transfer in fusion (Wang and Li, 2011).

2. CASE STUDY, DATA AND METHODOLOGY

2.1. Study Data

The study materials are cropped images from a set of simultaneously acquired, ortho ready WorldView2 panchromatic and multispectral images, acquired on June 3, 2012, around 11:30am. The original images show an area around the Turkish province of Trabzon. The cropped images used in this study show an area around the Sürmene district.

The placement of Trabzon within Turkey is shown in Figure 2.1. In Figure 2.2, a map of Trabzon province is shown, displaying the districts including Sürmene.

Figure 2.1. Trabzon province marked red on a map of Turkey (URL-6, 2012)

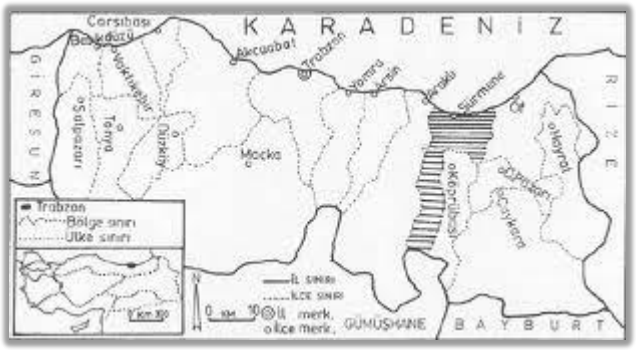

Figure 2.2. Trabzon province with its districts (URL-7, 2012).

The multispectral images have eight bands with a GSD of 2m. The spectral ranges and name of the 8 multispectral bands are as listed in Table 2.1 (Padwick, et al., 2010). The panchromatic image has a GSD of 50cm. The ratio of resolutions is 4. The reported

spectral range of the panchromatic image is 450-800 nm; it covers the spectral ranges of bands 2-6, and intersects with the spectral range of band 7. Spectral radiance response graph is shown in Figure 2.3.

Table 2.1. Multispectral bands and spectral ranges (URL-3, 2012).

Name	Order	Range (nm)
Coastal	B1	400-450
Blue	B2	450-510
Green	B3	510-580
Yellow	B4	585-625
Red	B5	630-690
Red Edge	B6	705-745
Near IR 1	B7	770-895
Near IR 2	B8	860-1040

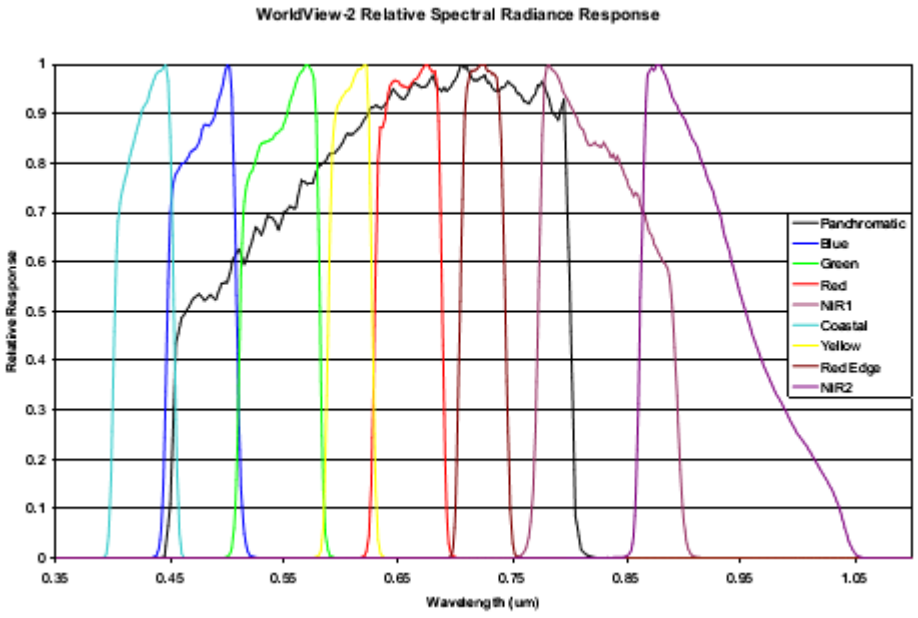

Figure 2.3. Spectral radiance responses (Padwick, et al., 2010).

Two well-aligned pairs of images are used as study material. Each pair consists of one panchromatic image and a multispectral image representing the same regions. The ratio of resolutions and sizes is 4 for all pairs. First panchromatic image is a 1568x1568 image representing an area of 768m x 768m. Second panchromatic image is a 1024x1024

image representing an area of 512m x 512m. The two panchromatic images and the upsampling of the two multispectral images are shown in Figure 2.4.

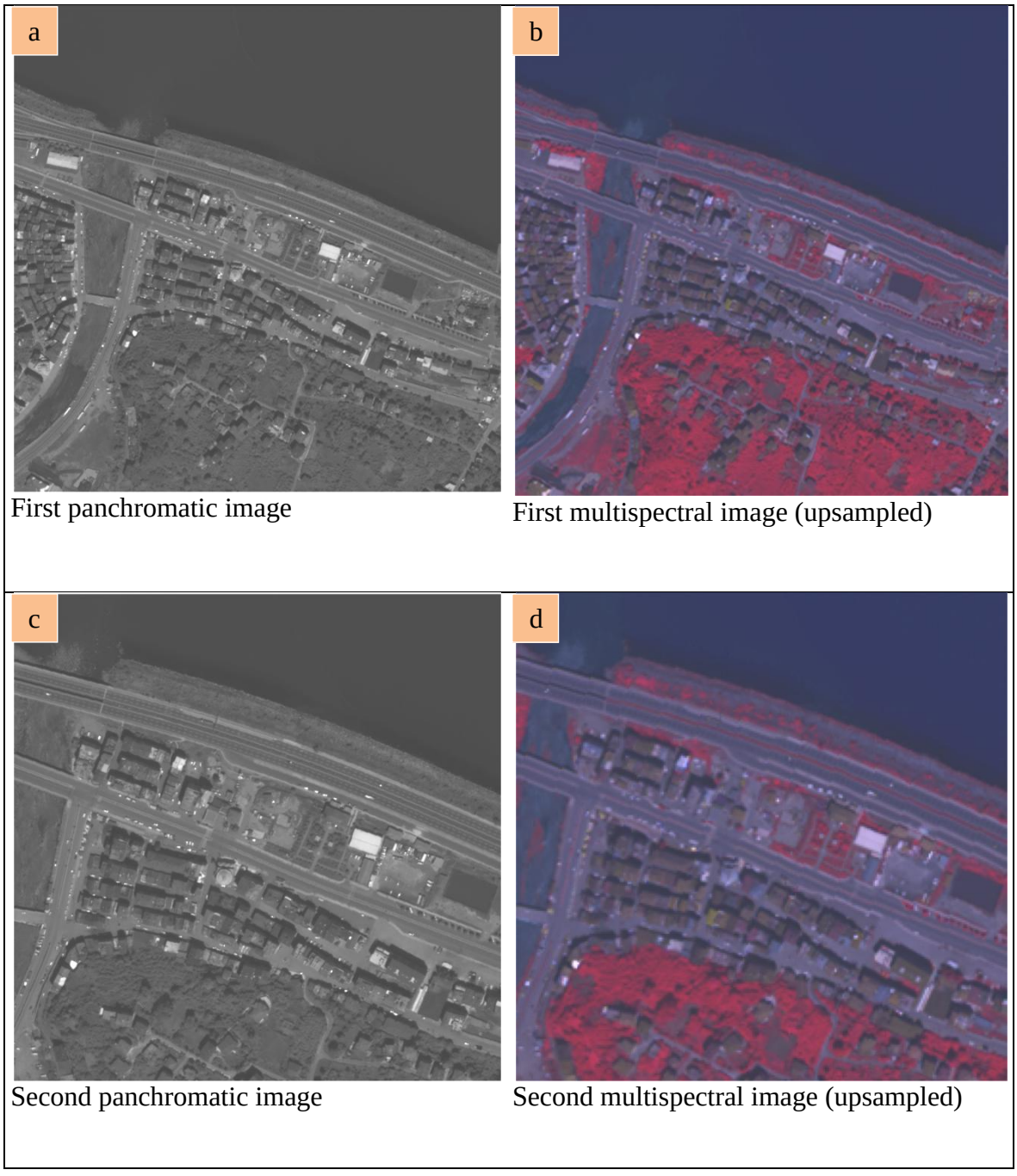

Figure 2.4. Input image pairs

The band combination used to display multispectral images is [7,5,3] (NIR1, Red, Green). The images are followed by Tables 2.2., and 2.3., listing correlation information

between eight bands of the upsampled multispectral image and the panchromatic image. First two multispectral bands have low correlation with the last two multispectral bands.

Table 2.2. Correlation statistics for the first image pair

	P	**B1**	**B2**	**B3**	**B4**	**B5**	**B6**	**B7**	**B8**
P	1.0000	0.7171	0.7120	0.7719	0.8572	0.8616	0.8240	0.6307	0.6214
B1	0.7171	1.0000	0.9304	0.9072	0.9016	0.8367	0.4152	0.0966	0.1022
B2	0.7120	0.9304	1.0000	0.9688	0.8552	0.8665	0.3717	0.0870	0.0694
B3	0.7719	0.9072	0.9688	1.0000	0.8805	0.8927	0.4713	0.2064	0.1816
B4	0.8572	0.9016	0.8552	0.8805	1.0000	0.9406	0.6638	0.3456	0.3543
B5	0.8616	0.8367	0.8665	0.8927	0.9406	1.0000	0.6554	0.3790	0.3575
B6	0.8240	0.4152	0.3717	0.4713	0.6638	0.6554	1.0000	0.8980	0.9087
B7	0.6307	0.0966	0.0870	0.2064	0.3456	0.3790	0.8980	1.0000	0.9668
B8	0.6214	0.1022	0.0694	0.1816	0.3543	0.3575	0.9087	0.9668	1.0000

Table 2.3. Correlation statistics for the second image pair

	P	**B1**	**B2**	**B3**	**B4**	**B5**	**B6**	**B7**	**B8**
P	1.0000	0.7667	0.7748	0.8166	0.8638	0.8646	0.8224	0.6306	0.6199
B1	0.7667	1.0000	0.9248	0.9013	0.9171	0.8495	0.5424	0.2252	0.2361
B2	0.7748	0.9248	1.0000	0.9689	0.8751	0.8942	0.5094	0.2366	0.2165
B3	0.8166	0.9013	0.9689	1.0000	0.8941	0.9153	0.5882	0.3403	0.3088
B4	0.8638	0.9171	0.8751	0.8941	1.0000	0.9318	0.7281	0.4108	0.4249
B5	0.8646	0.8495	0.8942	0.9153	0.9318	1.0000	0.7059	0.4465	0.4169
B6	0.8224	0.5424	0.5094	0.5882	0.7281	0.7059	1.0000	0.8772	0.8941
B7	0.6306	0.2252	0.2366	0.3403	0.4108	0.4465	0.8772	1.0000	0.9494
B8	0.6199	0.2361	0.2165	0.3088	0.4249	0.4169	0.8941	0.9494	1.0000

The panchromatic image has the worst correlations with images of multispectral band eight compared to images of other multispectral bands. This is within expectations, as the spectral range of the panchromatic image does not even intersect with the spectral range of the eighth band. Among the consecutive bands of the multispectral image, the

fifth and sixth band images have lower correlation; the other consecutive bands have high correlation. The highest correlations are between images of bands two and three, and between images of bands seven and eight. Band 3 (Green) images have low correlations with the images of near infrared bands seven and eight.

IWSSIM values between the panchromatic image and the mean of the bands of the upsampled multiplicative image are 0.7057 for pair 1, 0.6956 for pair 2.

The spectral range of the panchromatic image does not intersect with the spectral ranges of the first band (coastal) and eighth bands (NIR-2). IWSSIM values between the panchromatic image and the mean of the bands 2-7 of the upsampled multiplicative image are 0.7257 for pair 1, 0.7123 for pair 2.

2.2. Methodology

Using a co-registered pair of a panchromatic image and a multispectral image for the same region on Earth, the methodology is as described below and in Figure 2.5. Fusing the input images, first, three components are created, namely the spectral component, the spatial component and the flexibility component. These components are described by certain criteria in general. In this study, certain techniques are devised and used in creation of these components, along with already existing techniques satisfying these criteria.

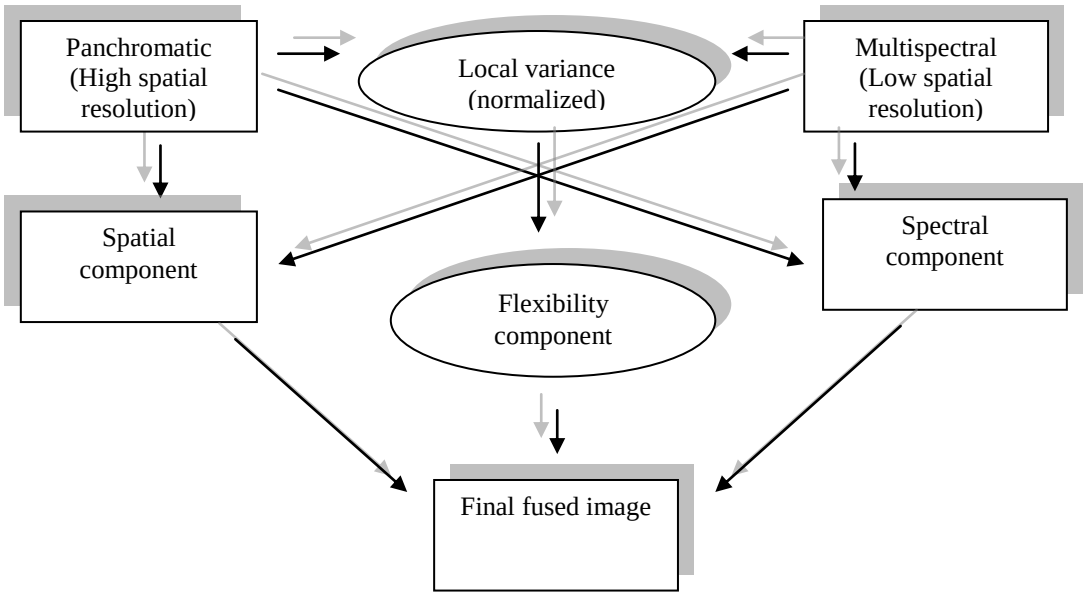

Figure 2.5. Flow chart of the methodology

The first component is the spectral component. The spectral component is an image with the same GSD as the input panchromatic image. The spectral range and the number of bands are the same as the input multispectral image. Furthermore, the spectral component is to satisfy two more criteria that are introduced below.

1) After downsampling, the resulting image needs to be (approximately) equal to the input multispectral image {Pradhan, 2006 #257}.
2) log (IWSSIM before spectral fusion) / log (IWSSIM after spectral fusion) is bigger than a threshold.

Wavelet based techniques produce spectrally well fused images, candidates for the spectral component. Two new candidates for spectral component, one based on covariances, and one based on least squares are devised and used.

The spectral components should serve well as a final product in many civilian applications. Further information is given in Section 2.2.1. The spectral components are spatially enhanced with the final fusion described in Section 2.2.3.

Other than the wavelet method and the two proposed methods, spectral enhancements of other methods, as explained in Section 2.2.1.3., are also candidates for the spectral component, as they satisfy the first criterion.

The second component is the spatial component. Like the spectral component, the spatial component is an image with the same GSD as the input panchromatic image, and the spectral range and the number of bands are the same as the ones of the input multispectral image.

Scalar multiples of images have (approximately) the same spatial content. A building is a building whether it is dark outside or it is brighter. An image whose bands are multiples of the input panchromatic image has the same spatial content with the input panchromatic image.

Furthermore, one should be able to modify the panchromatic image as well, without losing desired details. A vector space approach is used. A vector space of images describing non-desired details is defined.

The vector space is the space of images that contain only the not desired details, the details that are allowed to be discarded or freely added afterwards. This vector space is used in defining the seminorm and subsequently the semi-inner product. The seminorm is defined such that any element of this vector space has a seminorm of zero.

The bands of the spatial component are some scalar multiples of images whose difference with the input panchromatic image lies in this vector space of undesired details. Spatial content should be preserved. Depending also on the choice of the coefficients defining these multiplicities, the spectral content will be enhanced. Eight alternatives are presented and compared against each other. Further discussion is in section 2.2.2.

Last component of the triple fusion is the flexibility component. The flexibility component is an image that looks like a more continuous version of the edge images of the input images.

First, the local variances are computed. When the ratio of resolutions is four, the chosen size of windows for local variance computation is 5x5, as in (Gungor, 2008); five is the smallest odd integer strictly bigger than the ratio of resolutions. In a local variance image, each pixel value is the variance of the window centered around that pixel in the original image. The local variance image is normalized by its maximum attained value. The values are between zero and one.

Afterwards, a flexibility function series is chosen (eg. (19) or (20)). Additionally, the flexibility parameter is chosen. If the flexibility parameter is close to zero, the final fused image will look more like the spatial component, and if the flexibility parameter is close to one, the final fused image will look more like the spectral component.

The chosen flexibility function is applied entry-wise to the normalized local variance image, also amplifying the edges. The resulting image is the flexibility component. The final fused image is a convex combination of the spatial and spectral component, where the coefficients are defined by the flexibility component.

2.2.1. Spectral Component

A spectrally well fused image should be such that when downsampled, one gets the original multispectral image, or very close to the original multispectral image. This corresponds to Wald's first property (Pradhan, et al., 2006; Wald, et al., 1997). The hypothetical optimal fused image should satisfy this property. Haar wavelet fused images satisfy this, but fused images obtained by applying some other prevalent fusion methods, like PCA or IHS methods, do not satisfy this property.

Any spectrally well fused image is a candidate for the spectral component. The spectral component is a spectrally well fused image that also preserves a predefined level

of spatial details. The corresponding upsampling of the original multispectral image is also a spectrally well fused image, but not a spectral component.

The spatial structure of the spectral component should resemble the panchromatic image much better than an upsampling of the original multispectral image. The level of resemblance is given by the SSIM and IWSSIM values (section 1.5.). The maximal and optimal values are 1. A successful fusion increases the IWSSIM and SSIM values towards one. The following spatial criterion has been set for the spectral component in addition to being a spectrally well fused image.

- log (IWSSIM before spectral fusion) / log (IWSSIM after spectral fusion) is bigger than a threshold.

The desired level of IWSSIM by the author is the square root of the IWSSIM values before the spectral enhancement, so the set threshold is two. For instance, if the IWSSIM between the upsampled multispectral bands and panchromatic image is bigger than 0.64, then the IWSSIM values after the spectral enhancement need to be bigger than 0.8. Also, square root of a number is the geometric mean of that number with one, where one is the optimal value for IWSSIM. Thresholds between two and three serve well, but a threshold set at four turns out to be very restrictive.

In addition to already existing Haar wavelet technique, two techniques creating spectrally well fused images, hence candidates for the spectral component, are introduced. These are compared against each other and other techniques.

In many fusion methods, an upsampling like nearest neighbor upsampling of the original multispectral image is used in the creation of the fused image. The fused image is to have similar spectral properties with the original multispectral image, hence also its upsampling, and at the same time should carry the spatial details of the original panchromatic image, as much as possible. The aforementioned spectrally well fused images can be considered as better replacements of the upsampling, a replacement that is spatially closer to the desired fused image and the original panchromatic image. One may consider these spectrally well fused images as high resolution upsampling, ones that are created using both the original multispectral image and the original panchromatic image, or another spatially good image and carry an adequate portion of the spatial details in the original panchromatic image not existent in the original multispectral image. The spectrally well fused images should be able to serve good enough as a final product in many cases.

Two fusion techniques are introduced below. They satisfy the first criterion, and hence are candidates for spectral component along with the Haar wavelet technique introduced in Section 1.4.1.2.

2.2.1.1. Covariance Based Spectrally Well Fused Image

Like many other prevalent methods, this method starts with upsampling the multispectral image. Also, another spectrally well fused image may be used, instead of the upsampling.

The panchromatic image is normalized by its standard deviation. For each band, the normalized panchromatic image is multiplied with its covariance with the upsampling of the multispectral image. The resulting image is the corresponding band of the first intermediary image. Now, each band of the first intermediary image is a multiple of the panchromatic image.

The second intermediary image is the first intermediary image minus the upsampling of the multispectral image. The second intermediary image is downsampled and then upsampled, to obtain the third intermediary image. This will ascertain that when downsampled, the second and third intermediary images yield to the same image.

The fourth intermediary image is the difference between the third intermediary image and the second intermediary image. When the fourth intermediary image is downsampled, the zero image will be obtained.

The fused image is the sum of the fourth intermediary image and the upsampling of the multispectral image.

When the resulting fused image is downsampled, the original multispectral image will be obtained.

This method of spectrally well fused image creation can be applied iteratively. Instead of the panchromatic image, one can use another spatially good image.

If a low-low wavelet decomposition (denote by W) is used for the downsampling, we have the following:

Let λ_i be such that λ_i times the panchromatic image is the i^{th} band of the first intermediary image. Let $Q=W^{-1}(W(panchromatic\ image))$, $R=panchromatic\ image-Q$. Then we have $W(R)=zero\ image$.

Let $x_i = W(X_i)$ be the i^{th} band of the original multispectral image, and $X_i = W^{-1}(x_i)$, i^{th} band of the upsampling. Then second intermediary image equals the third intermediary image plus the fourth intermediary image, where the i^{th} band of the third intermediary image equals $\lambda_i Q - X_i$, and the i^{th} band of the fourth intermediary image equals $\lambda_i R$.

The i^{th} band of the final fused image equals $\lambda_i R + X_i$. When downsampled, the original multispectral image will be obtained. Any multispectral image of adequate size has wavelet decomposition, so the hypothetical ideal fused image, as well. The detail parts in the wavelet decomposition is estimated using covariances.

Figure 2.6. shows the covariance based spectrally well fused image (in Figure 2.6.c)) obtained for a given pair of panchromatic image (in Figure 2.6.a)) and multispectral image (upsampled version in Figure 2.6.b)). The cars and other small objects become distinguishable from their surroundings. The colors have been preserved. Visually, it seems to be a good candidate for a spectral component. Spatial enhancements will be done later that will further enhance the spatial details, compared to the upsampled multispectral image, but causing some small spectral distortion.

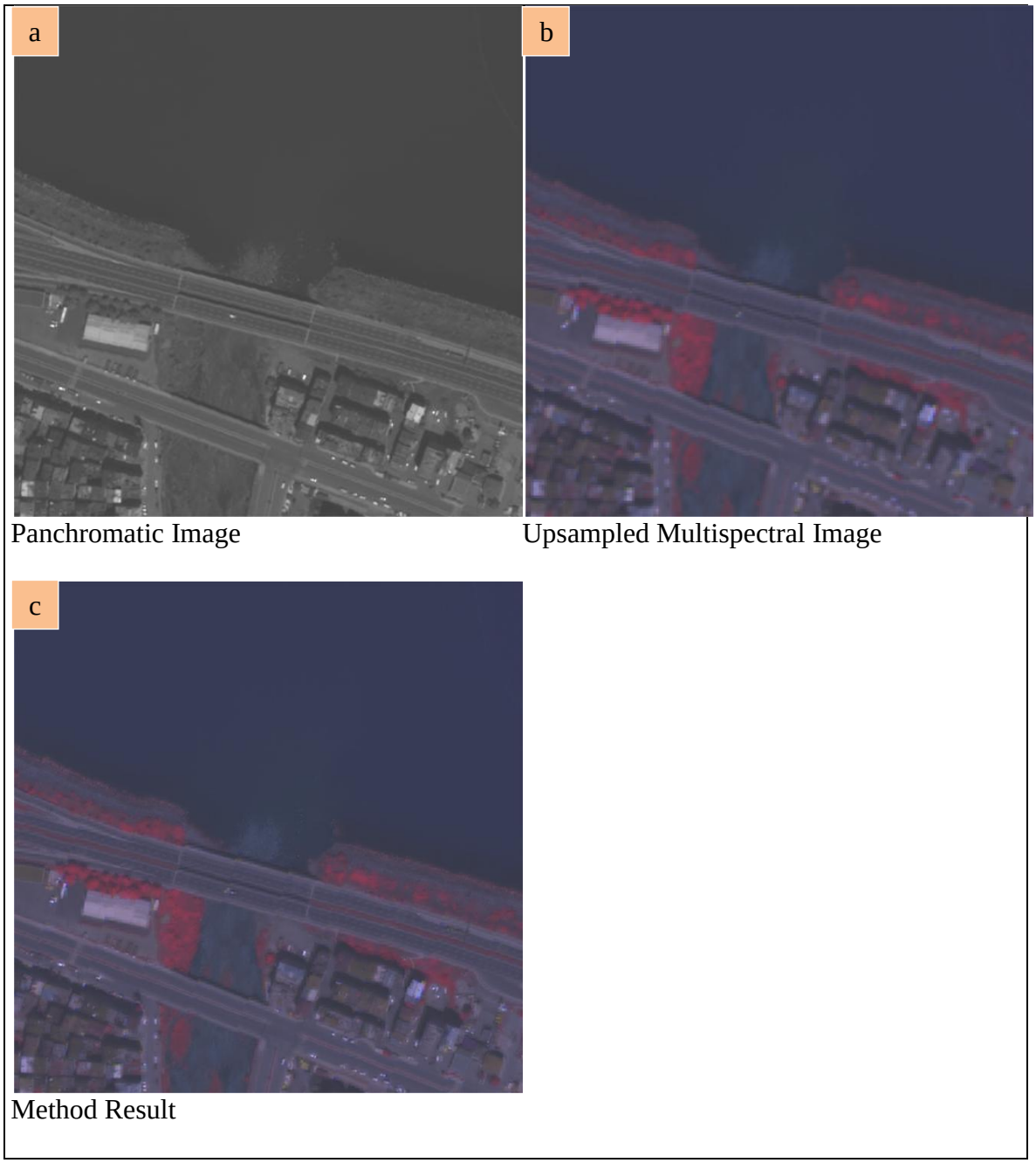

Figure 2.6. Covariance based method image example (zoomed)

2.2.1.2. Least Squares Based Spectrally Well Fused Image

First, a basic upsampling is created which can be the nearest neighbor upsampling, or some existing spectrally good image. Each band of the basic upsampling and the panchromatic image are reshaped as vectors (concatenating column vectors). Least squares

estimation coefficients λ_i are calculated. With these coefficients, the difference between two sides of (27) has the smallest 2-norm.

$$Pan \approx \sum_i (\lambda_i * i^{th}\ upsampled\ multispectral\ band) \quad (27)$$

Panchromatic image is approximated by the sum of λ_i times upsampled multispectral bands, and the difference has the smallest 2-norm possible. More than one set of the coefficients may give rise to the same 2-norm for the difference.

Negative coefficients may be allowed or one may force positive coefficients in the least squares estimation (increasing the 2-norm of the difference). The latter has been chosen.

After the calculation of the least squares coefficients, an intermediary single band image is created. This image is downsampled and then upsampled by nearest neighbor method. The first difference image is the image that is the difference between the original panchromatic image and the intermediary single band image. The second difference image is a multispectral image where each band is a multiple of the first difference image, the factor given by least squares coefficients. The second difference image is added to the basic upsampling to get the spectrally good image. The method can be applied iteratively. A spectrally well fused image may be used instead of upsampling, and a spatially good single band image may be used instead of the panchromatic image.

Figure 2.7. shows the least squares based spectrally well fused image (in Figure 2.7.c)) obtained for a given pair of panchromatic image (in Figure 2.7.a)) and multispectral image (upsampled version in Figure 2.7.b)).

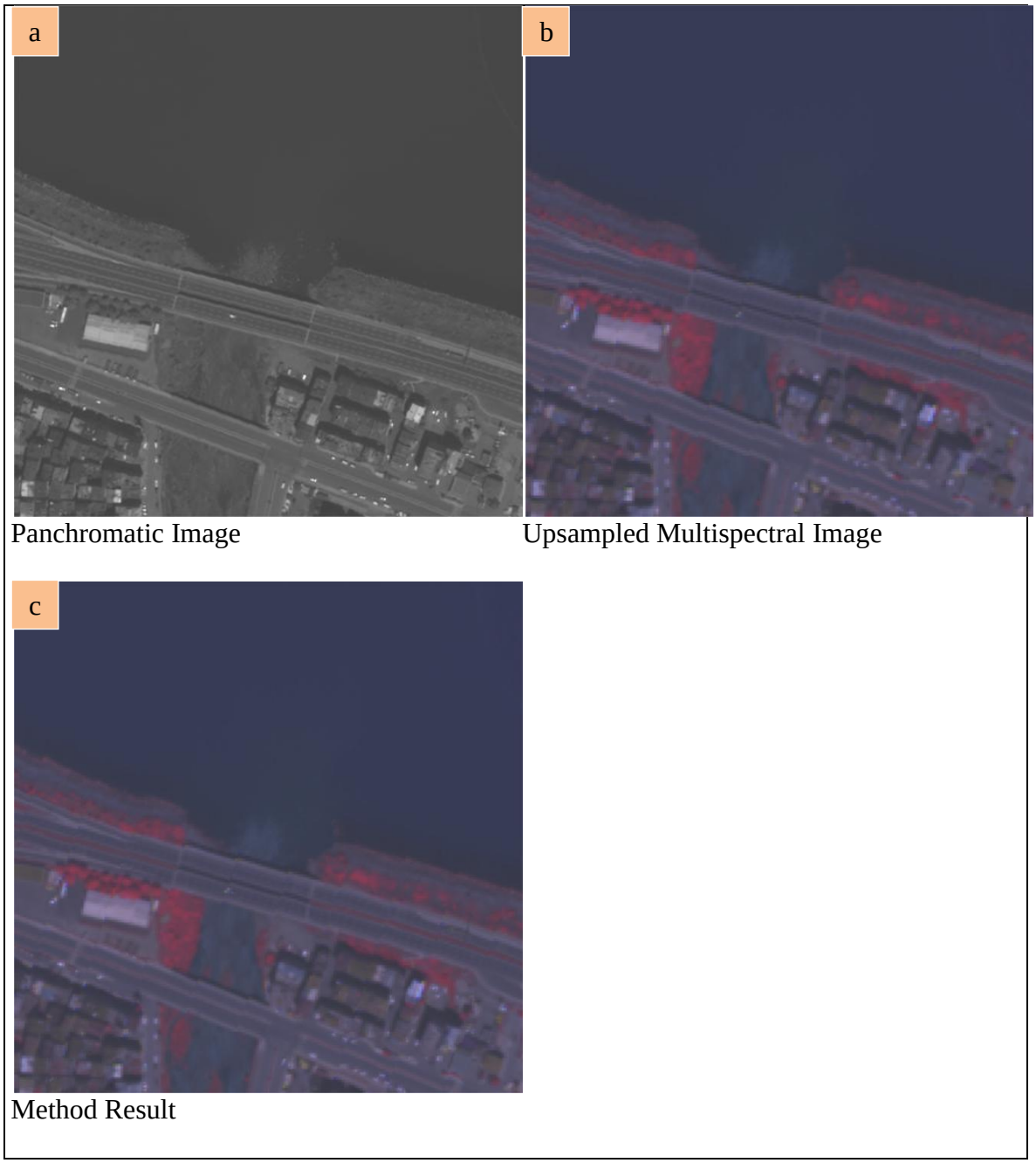

Figure 2.7. Least squares method image example (zoomed)

2.2.1.3. Modification for Spectral Enhancement

IHS, PCA and Brovey methods fail Wald's first property. When the fused image is downsampled, one does not get the original multispectral image. The artifacts can be removed to make the fused image a proper upsampling of the original multispectral image. A linear approach is preferred in this study.

With scalar multiplication, mean values are equalized. The difference between downsampled fused image and the original image is upsampled. This upsampling is subtracted from the fused image. An example is shown in Figure 2.8.

A multiplicative approach can also be used. For instance, first the function log(1+x) may be applied term by term, and the linear approach above can be applied to the result, followed by term by term exponentiation.

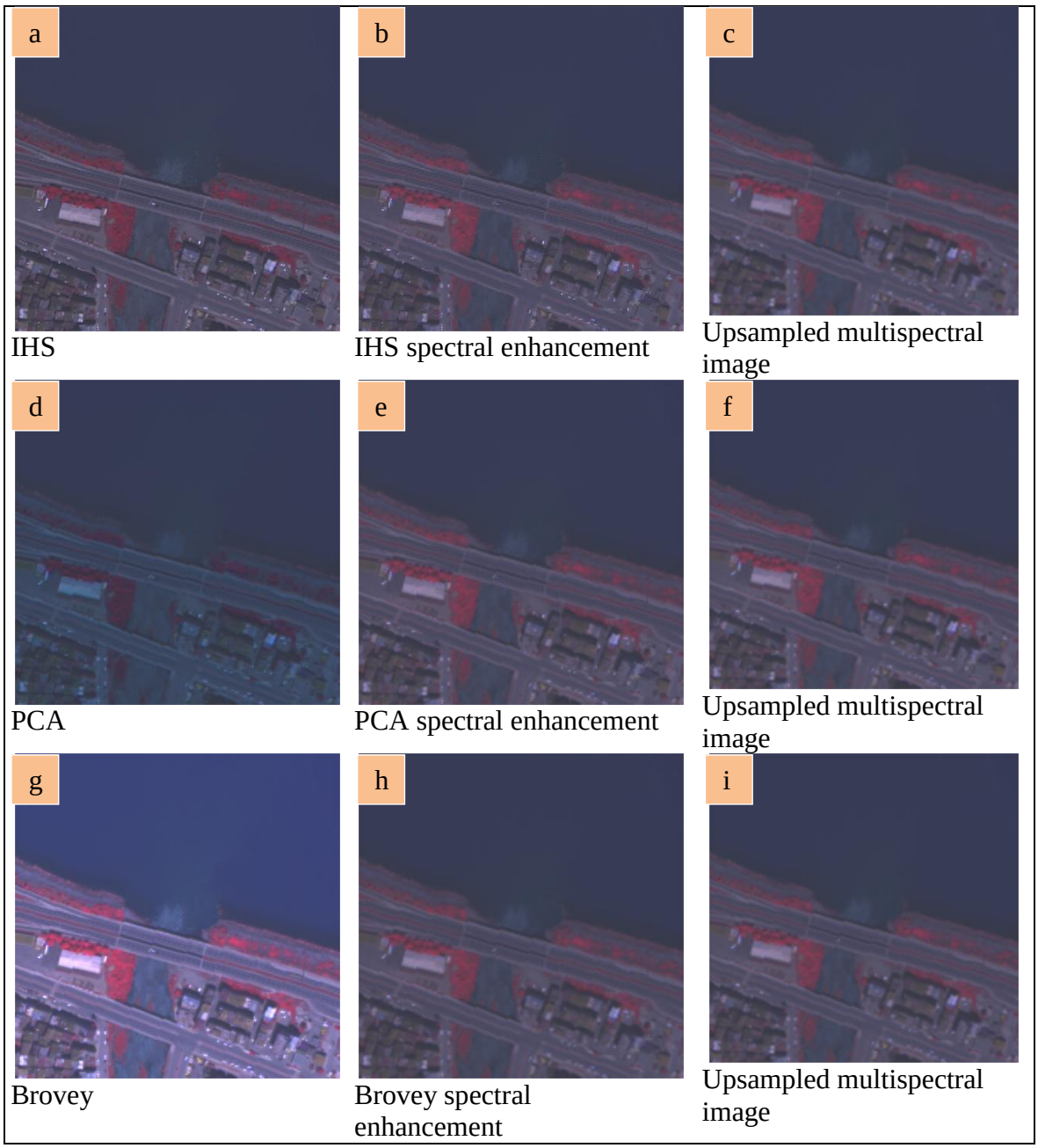

Figure 2.8. Spectral Enhancement

2.2.2. Spatial Component

"Not all pieces of information are fusion-worthy" (Hossny, et al., 2008). A vector space approach is used to manage pieces of spatial detail information that are fusion-worthy. A vector subspace of images, labeled T, within the image space is defined to be used to describe information that can be discarded on the panchromatic side. Afterwards the calculations are done in the complement of T within the whole image space. The ideal T space would be a subspace of the images that have zero covariance with the bands of the hypothetical ideal fused image. To make this less image dependent, one needs to go to subspaces.

The bands of the hypothetical ideal fused images constitute a hyperplane, a subspace of the image space endowed with the inherited seminorm, semi-inner product pair. Each hyperplane has a complement with a big dimension, and the common complement is expected to be non-zero in many interesting cases, for scenes of particular environment types. The rationale is that the Earth and the remote sensing images are not completely chaotic. Rectangular and elliptical shapes appear often in remote sensing images of for instance urban environments, forests and their mixtures. If it were chaotic, such regular shapes would appear as likely as any other random shape. The ideal T is the common complement of the related hyperplanes. In reality, the hypothetical ideal fused images are not available; otherwise there wouldn't be any need for fusion. Instead of the ideal image, there is a multispectral downsampling whose bands lie in the downsampled hyperplane, and there is a panchromatic image related to that ideal image, that is expected to be close to the original hyperplane. The panchromatic image will be projected onto the hyperplane.

This discussion relates to the manipulation using convolution filter kernels with the kernel spaces of the convolution. Using the vector space approach here gives some freedom as opposed to the common convolution based approach, where all or none of the whole kernel space is taken by choosing a filter kernel. For instance, one may choose to exclude the image where all the entries are one from the space T, but eliminating that image would not be directly possible in an edge convolution based approach. One may add, delete, or otherwise modify the basis elements with this vector space based approach, in order to get the closer to the ideal T space.

It is not necessary that the vector space T is defined using edge kernels, but it is more practical. In practice, the following procedure is recommended.

1) Choose a filter sequence. Let T_{max} be the subspace generated by the kernel spaces of these filters. So, for any element in T_{max}, the zero image is obtained, when that element is valid convolved with at least one filter in the sequence. T will be a subspace of T_{max}.
2) Choose a threshold for the ratio of change in the panchromatic image compared to the mean radiance of the panchromatic image.
3) Among the subspaces of T_{max} that cause a change in panchromatic image below the threshold, T is one that has the biggest dimension.

In this study, a small change T space (0.5% threshold) is used, which is assumed to work as a reconstruction from quantization (Pratt, 2001). It can also serve for compression, as the dimension of the complement is lower than the dimension of the whole image space. In other applications, a larger T space with bigger dimension can be used.

With the T space used in this study, the elements have zero valid convolution with the symmetric part of the horizontal and vertical Sobel kernels. As opposed to convolution based approaches with kernels, this vector space approach gives more freedom; the vector space does not need to be the full kernel space of convolution kernels. It can be made smaller, larger, or otherwise different.

The part of the panchromatic image in T has a maximal attained value of 1.8, so approximately 0.5% of the mean radiance of the panchromatic image, lower than 3%, typical bound used in ERGAS comparisons. This result was not unexpected, as the space T has been chosen to cause changes less than 0.5%. The restriction of preserving spatial details would let the percentage go a bit higher. This can be easily done, for instance deleting some basis elements.

Sample composite images from elements of T are shown in Figure 2.9. Certain + and x type figures appear, but the edges will be zero. Figure 2.10. shows the binary edge images of the panchromatic image and its part in the complement of T. No visible change occurs in high frequency details.

Any T space should contain the fully noisy image, the checkerboard image, where the only pixel intensity values attained are 0 and 1, and these are attained alternatingly. The image in Figure 2.9.a) is a multiple of a fully noisy image.

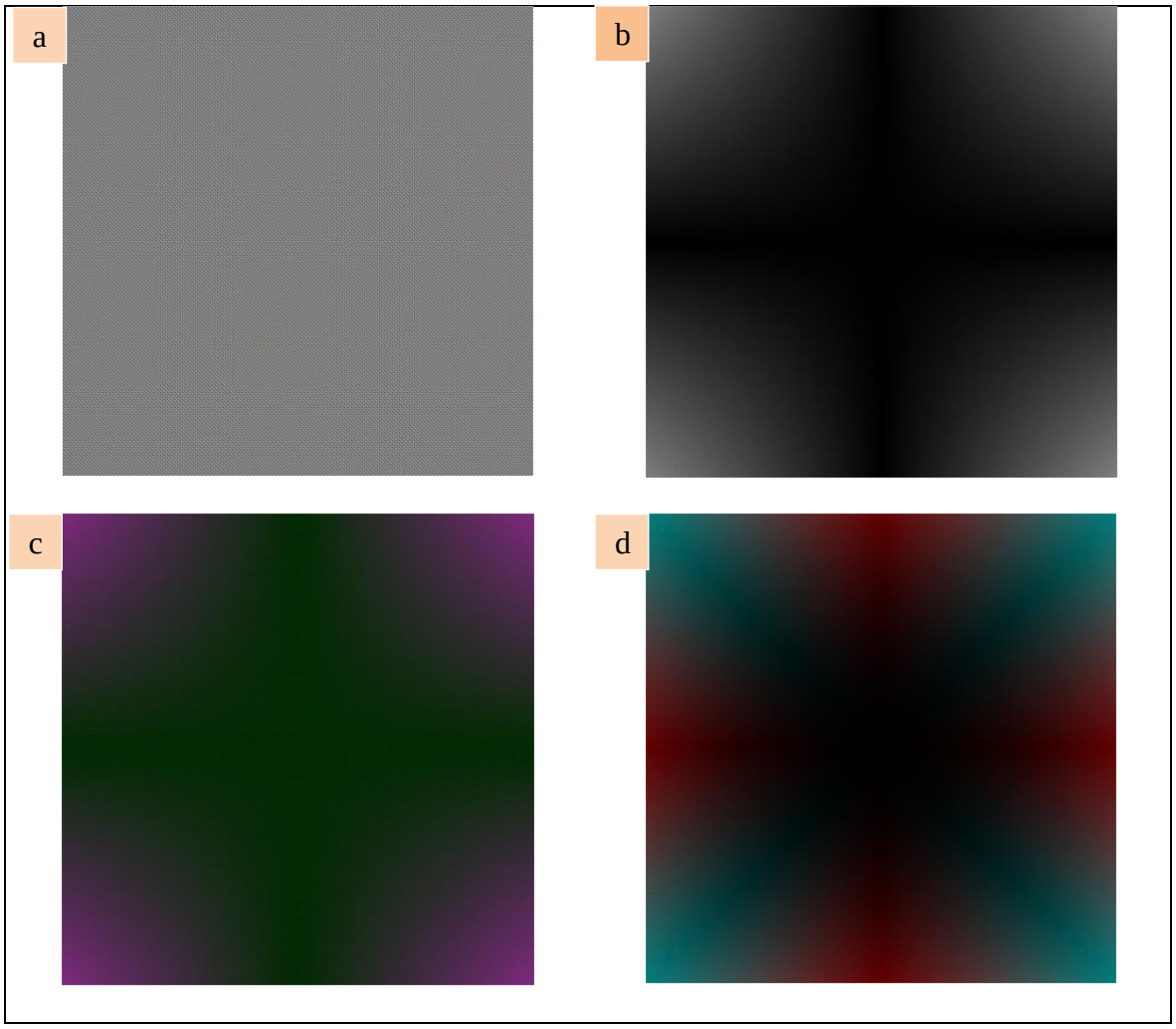

Figure 2.9. Four composite images each from three images in T

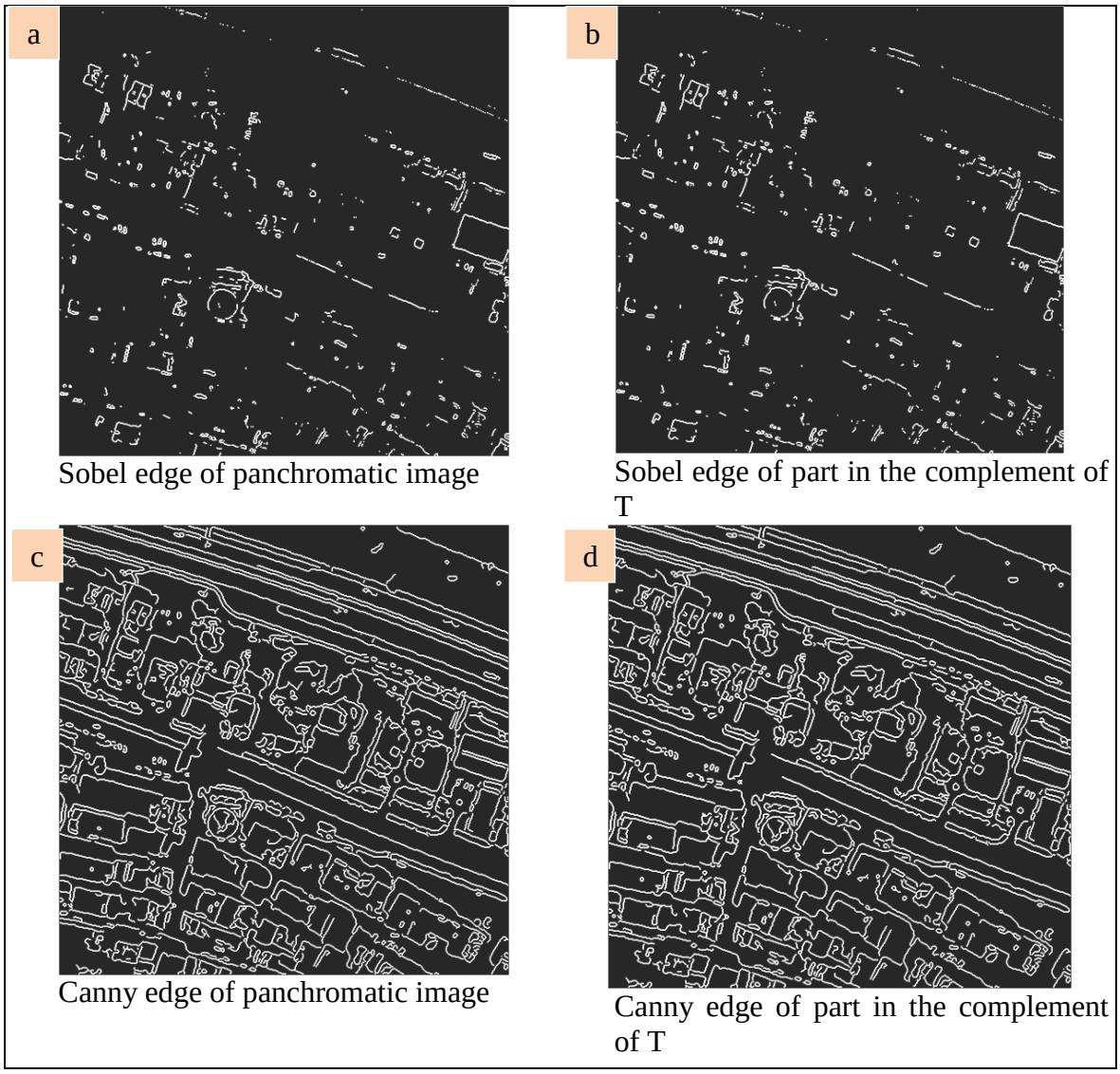

Figure 2.10. Binary edge images of the panchromatic image 3, and its part in the complement of T

After the choice of the T space, using T as a kernel space, and variance/covariance of images, a seminorm and semi-inner product is defined. First, a basis of T is found, where each basis element has zero covariance with the others. Furthermore, the basis elements are normalized to have a unit variance.

The used seminorm is the seminorm associated with the quotient norm of the image space over T in the Noetherian way. If an image has zero covariance with all the basis elements, its norm is square root of its variance. If the image has non-zero covariance with any basis element, first that part in T is removed, and then the variance is calculated as in (28).

$$\|A\| = \sqrt{Variance(A - \sum_{t=basis\ element} Covariance(A,t) * t)} \quad (28)$$

The semi-inner product is the semi-inner product associated with this seminorm. The non-negativity and homogeneity are obvious. Triangle inequality will be proved with (29) and the following discussion.

Let $A=C+t$, $B=D+s$, be two images, where t, s are in T, and C, D are in the complement of T with zero mean.

$$\|A+B\|^2 = \|A\|^2 + \|B\|^2 + 2\,\|A\|\|B\|Correlation(C,D) \leq (\|A\| + \|B\|\,)^2 \quad (29)$$

Taking square roots we get the triangle inequality. Correlation is between -1 and 1, inclusively.

Likewise (30) holds.

$$\|A-B\|^2 = \|A\|^2 + \|B\|^2 - 2\,Correlation(C,D)\,\|A\|\|B\| \quad (30)$$

Therefore, the parallelogram identity holds.

An intermediary image is created to be used in spatial enhancement. The bands of the intermediary image lie in the orthogonal complement of T, and the seminorm of their difference with the image whose each band is some multiple of the panchromatic image is zero.

In this study, the coefficients have been chosen in eight different ways:

1) Covariance of the band with the panchromatic image normalized by the variance of the panchromatic image
2) Reciprocal of the covariance of the band with the panchromatic image
3) Ratio of the mean radiance of the band over the mean radiance of the panchromatic image
4) Ratio of the standard deviation of the band over the standard deviation of the panchromatic image
5) Ratio of the standard deviation of the band over the standard deviation of the panchromatic image and shifted to match the means
6) Least squares approximation coefficients

7) Least squares approximation coefficients forced to be nonnegative
8) Equal weight.

2.2.3. Final Fusion

The final fused image is a convex linear combination of the spatial and spectral components. The coefficients of the combination depend on the flexibility component that is defined using the local variances. If a linear approach is used, we have the relation described in (31), where the flexibility component and the final fused image depend on a flexibility parameter r.

$$\text{Final Fusion} = (\text{Spatial C} - \text{Spectral C}) * \text{Flexibilty C} + \text{Spectral C} \quad (31)$$

Around the regions with high local variance, the fused image will look more like the spatial component, hence the panchromatic image, and where the local variances are small, the fused image will resemble the spectral component, hence the original multispectral image.

To construct the flexibility component, first the local variance image map is divided by the maximal attained value. Now the values are between 0 and 1. The flexibility component will not carry any neighborhood information, it will just depend on the local variance normalized intensity values. The dependence will be given by certain smooth functions that will be called flexibility functions. There will be some restrictions, other than that, the flexibility functions will be free, modifying the local variance image into the flexibility component in the desired way.

The intensity values of the flexibility component should stay in [0,1], and 0 should be mapped to 0, and 1 should be mapped to 1. So, the flexibility functions map unit interval to unit interval with fixed points at 0 and 1.

A larger local variance should translate to a larger value in the flexibility component, therefore the flexibility functions should be increasing.

To be able to apply Jensen type inequalities and to amplify the edges further, the functions should satisfy concavity conditions. If the flexibility functions are twice continuously differentiable, these conditions can be made simpler. A smooth convex function has nonnegative second derivative, and a smooth concave function has a

nonpositive second derivative. As the functions are increasing, the first derivative will be nonnegative.

The functions should depend on a parameter, changing the flexibility component r. As r approaches 0 and infinity, these functions should approach certain limit functions.

These limit functions are the floor function and the ceiling function, and they are not continuous. If the flexibility function is close to the floor function in (32), (large flexibility parameter r), the final fused image will look more like the spectral component. If the flexibility function is close to the ceiling function in (33), (flexibility parameter r close to 0), the final fused image will look more like the spatial component. This way the spatial enhancement of the spectral component will be determined.

$$floor(x) = \begin{cases} 0 & 0 \le x < 1 \\ 1 & x = 1 \end{cases} \tag{32}$$

$$ceiling(x) = \begin{cases} 1 & 0 < x \le 1 \\ 0 & x = 0 \end{cases} \tag{33}$$

The fused image depends among others on the choice of the spectral and spatial components, on the choice of the flexibility function and the flexibility parameter r.

Local variance image and flexibility component with function series (20), r=1/4, is computed for a grayscale Lena image. They are shown together with its Sobel edge in Figure 2.11. The flexibility component looks similar to an edge image, but with amplified edges.

Around the edges, the final image will be similar to the spatial component, and away from edges, it will be more similar to the spectral component.

In addition to linear combination, power means or multiplicative combinations as in (34) can be used.

$$\text{Final Fusion} = \left(\frac{1+\text{Spatial C}}{1+\text{Spectral C}}\right)^{\text{Flexibilty C}} * (1 + \text{Spectral C}) - 1 \tag{34}$$

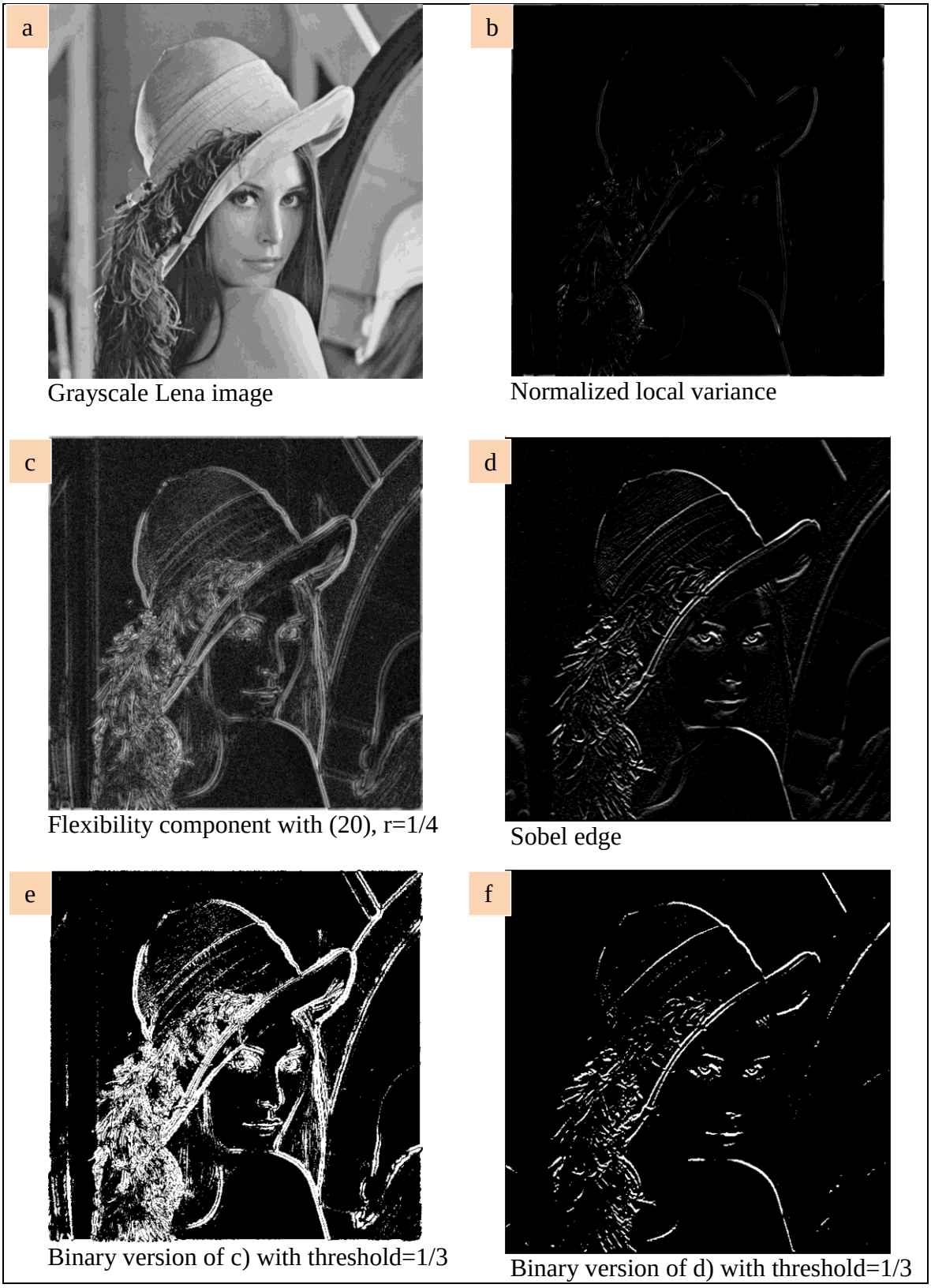

Figure 2.11. Flexibility component and local variance versus Sobel image

3. FINDINGS

3.1. A Comparison of Fusion Results with Downsampling First

The hypothetically ideal fused image won't be present in applications, but a simulation can be done, downsampling all the images, and comparing the fusion result to the original multispectral image, treating it like the hypothetically ideal fused image, the image that would be acquired, if the multispectral sensors of the satellite had the same spatial resolution with the panchromatic sensor.

Here, the input image pairs are downsampled first, and then these downsampling are fused together with the fusion techniques presented. Hypothetically, a good fusion technique should produce an image close to the original multispectral image. The fused images are compared with the original multispectral image from each pair, using MSE.

The MSE values are divided by the minimal MSE result occurred and presented in Table 3.1. The last column lists the geometric mean of these values for each fusion and input image pair, for better comparison. Best performer will have a value of 1, the others will have bigger values. The bold entries involve images obtained/modified by methods devised by the author.

Table 3.1. Normalized MSE values for the fusion of downsampled images, no spatial enhancement

Technique	Image pair 1	Image Pair 2	Geometric Mean
IHS	1.6678	1.6337	1.6507
PCA	14.3157	15.1228	14.7137
Haar	1.1972	1.2992	1.2472
Brovey	1.1920	1.2341	1.2129
Covariance based	**1**	**1**	**1**
Least Squares Based	**1.6079**	**1.7609**	**1.6827**
IHS Spectral Enhancement	**1.2113**	**1.2940**	**1.2520**
PCA Spectral Enhancement	**1.2329**	**1.1697**	**1.2009**
Brovey Spectral Enhancement	**1.9252**	**2.1224**	**2.0214**

The fused images are then spatially enhanced using each spatial enhancement configuration. The MSE values are calcul ated and then divided by the minimal one obtained among all fusion technique – spatial enhancement configuration combinations. Table 3.2 lists the results, again divided by minimal value, but only the best spatial enhancement configuration results are displayed for each fusion technique. Other spatial enhancements yielded larger, hence worse, values. Spatial configuration 3 has become the best one, for all but the PCA technique.

Table 3.2. Normalized MSE values for the fusion of downsampled images, best spatial enhancement configuration results

Technique	Config1	Image pair 1	Config 2	Image Pair 2	Geomean
IHS	3	1.4771	3	1.4455	1.4612
PCA	4	6.5111	4	6.2729	6.3909
Haar	3	1.1599	3	1.2074	1.1834
Brovey	3	1.2062	3	1.1861	1.1961
Covariance based	**3**	**1.0000**	**3**	**1.0000**	**1.0000**
Least Squares Based	**3**	**1.1212**	**3**	**1.1652**	**1.1429**
IHS Spectral Enhancement	**3**	**1.1668**	**3**	**1.2048**	**1.1856**
PCA Spectral Enhancement	**3**	**1.0278**	**3**	**1.0241**	**1.0260**
Brovey Spectral Enhancement	**3**	**1.2104**	**3**	**1.2672**	**1.2385**

Covariance based technique performed the best in all cases (Table 3.1. and Table 3.2.). Spectral enhancement improved PCA method performance greatly, but it worsened Brovey method's performance.

3.2. Choice of Coefficients for the Spatial Enhancements

Here, the performance of different spatial enhancement techniques are evaluated, applying them on only the original multispectral image. This, along with previous discussion will help choosing a spatial enhancement configuration to be applied to all the spectrally well fused images.

The second multispectral image is fused together with the intermediary spatially image Z for the third pair of input images with different coefficient configurations yielding different results. For CC, ERGAS and SID, these images are downsampled and then compared with the original multispectral image.

Fusion quality results are listed in Table 3.3. Images are shown in Figure 3.1. The best configuration will be used in all the final fusions with all the techniques, as the spatial improvements in other fusions should parallel the spatial improvements in the upsampled multispectral image.

Table 3.3. Spatial coefficient configuration fusion quality statistics

Configuration	IWSSIM	SSIM	CC	ERGAS
1	0.8461	0.8293	0.0017	0.4304
2	0.8344	0.82	0.0023	0.9520
3	0.8497	0.8323	0.0041	0.7856
4	0.8484	0.8312	0.0034	0.6784
5	0.8488	0.8315	0.0037	0.7136
6	0.8517	0.834	0.006	1.3184
7	0.8371	0.8221	0.0023	0.7104
8	0.85	0.8326	0.005	0.9968

Configuration #6 (least squares configuration) is the best one spatially, closely trailed by configurations #8 and #3. Configuration #3 appears most frequently in Table 3.2, and also is one of the best ones in Table 3.2. Configuration #3 is chosen as the default spatial enhancement configuration.

In Figure 3.1, the multispectral image is enhanced spatially using the spatial coefficient configurations. None of the results are near desired levels. The roads and building in the chosen spatial enhancement configuration (configuration #3) seem sharper, compared to the other configurations, indicating better spatial enhancement, visually.

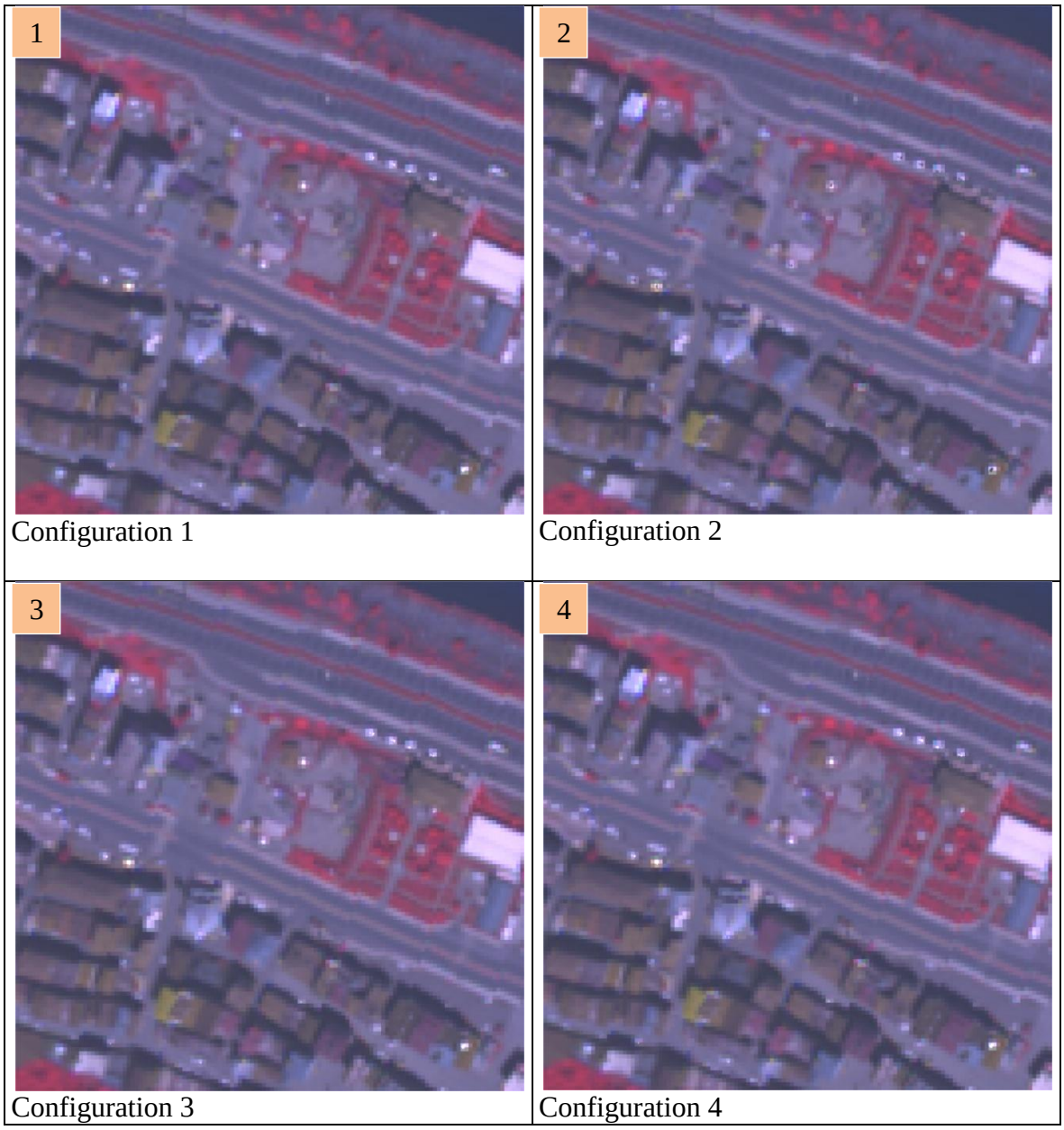

Figure 3.1. Images corresponding to different spatial coefficient configurations

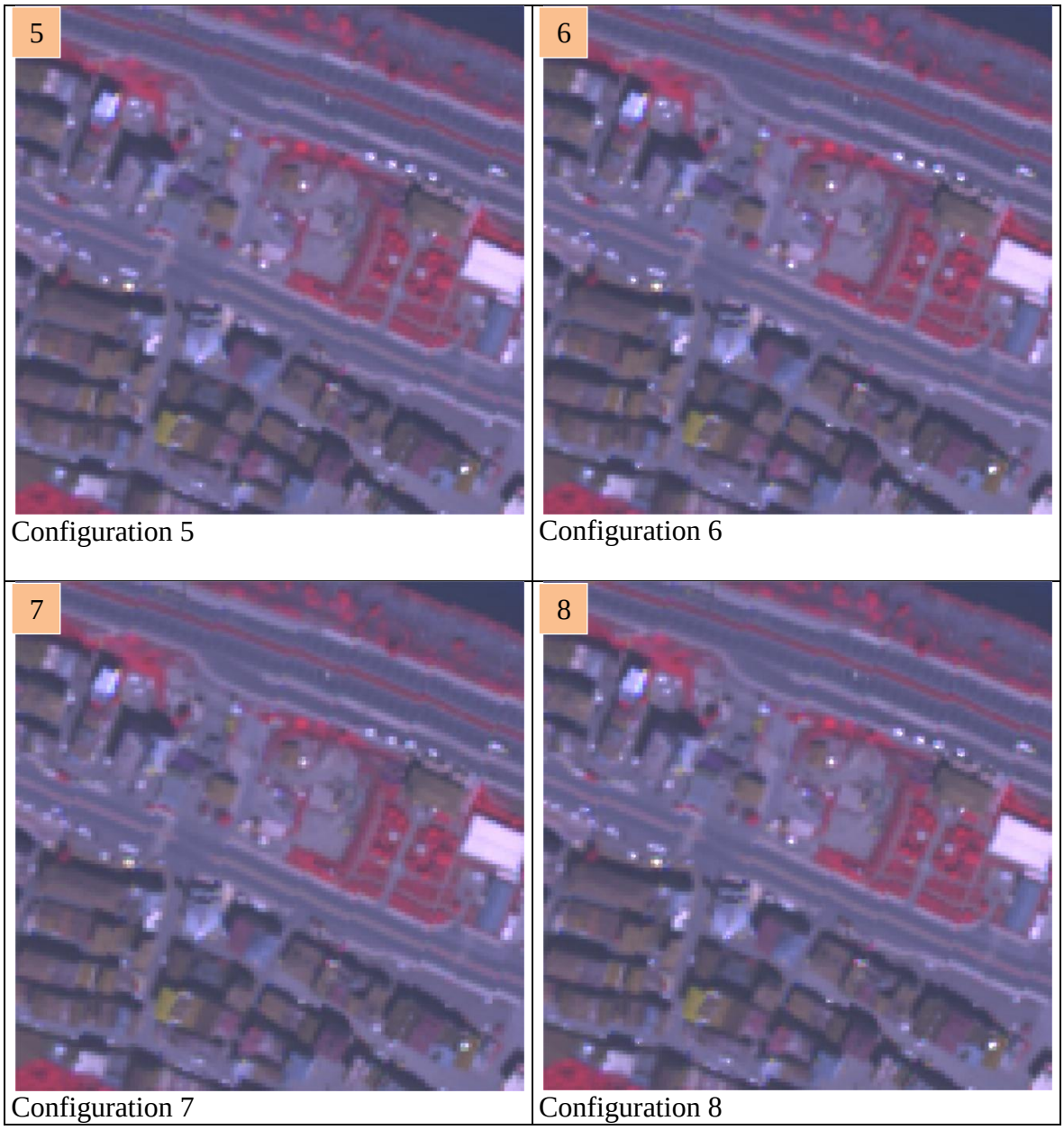

Figure 3.1. (continued) Images corresponding to different spatial coefficient configurations

3.3. Spectral, Spatial and Radiometric Quality Assessment Data

IHS, PCA and Brovey methods do not conform to the criterion that when downsampled, they become the original multispectral image, whereas the Haar wavelet method, and the two new methods presented do. For IHS, PCA and Brovey methods, the spectrally enhanced fused images are produced, as presented in Chapter 2.2.1.3. For all the nine images, the final fused images are obtained following the spatial enhancement procedure outlined in Chapter 2.2.2.

Here the assessment data will be presented. For each method, first the relevant images (result of the fusion, if needed the spectral enhancement, and the spatial enhancement) are shown along with the original multispectral image (upsampled) for visual spectral comparison in Figures 3.2., 3.3., 3.4., 3.5., 3.6., 3.7. They are followed by correlation statistics data in Tables 3.6., 3.9., 3.12., 3.15., 3.18., 3.21. The last rows are the sum of off-diagonal entries on that column.

Tables 3.4, 3.5., 3.7., 3.8., 3.10., 3.11., 3.13., 3.14., 3.16., 3.17., 3.19., 3.20, 3.22, 3.23. present the fusion quality results and radiometric statistics. The final fusion is done with f_r in (19) and the one in (20) with parameter r=1/4.

Table 3.4. Fusion metrics for the upsampled original multispectral image 1

IWSSIM	SSIM	CC	ERGAS	SID
0.8692	0.9557	0.0000	0.0000	0.0000

Table 3.5. Radiometric statistics for the upsampled original multispectral image 1

Diversity	Entropy	Thr_2.275%	MinMax	Contrast
10.4543	8.9941	[36,664]	[14,2047]	167.6058

3.3.1 IHS Method

The resulting images are shown in Figure 3.2. , and shown zoomed to the upper left quadrant in Figure 3.3. Spatial detail transfer is the very good, even better than the final enhancement. The enhancement worsened the fusion spatially. Spectrally, IHS did cause major color changes, especially around forests.

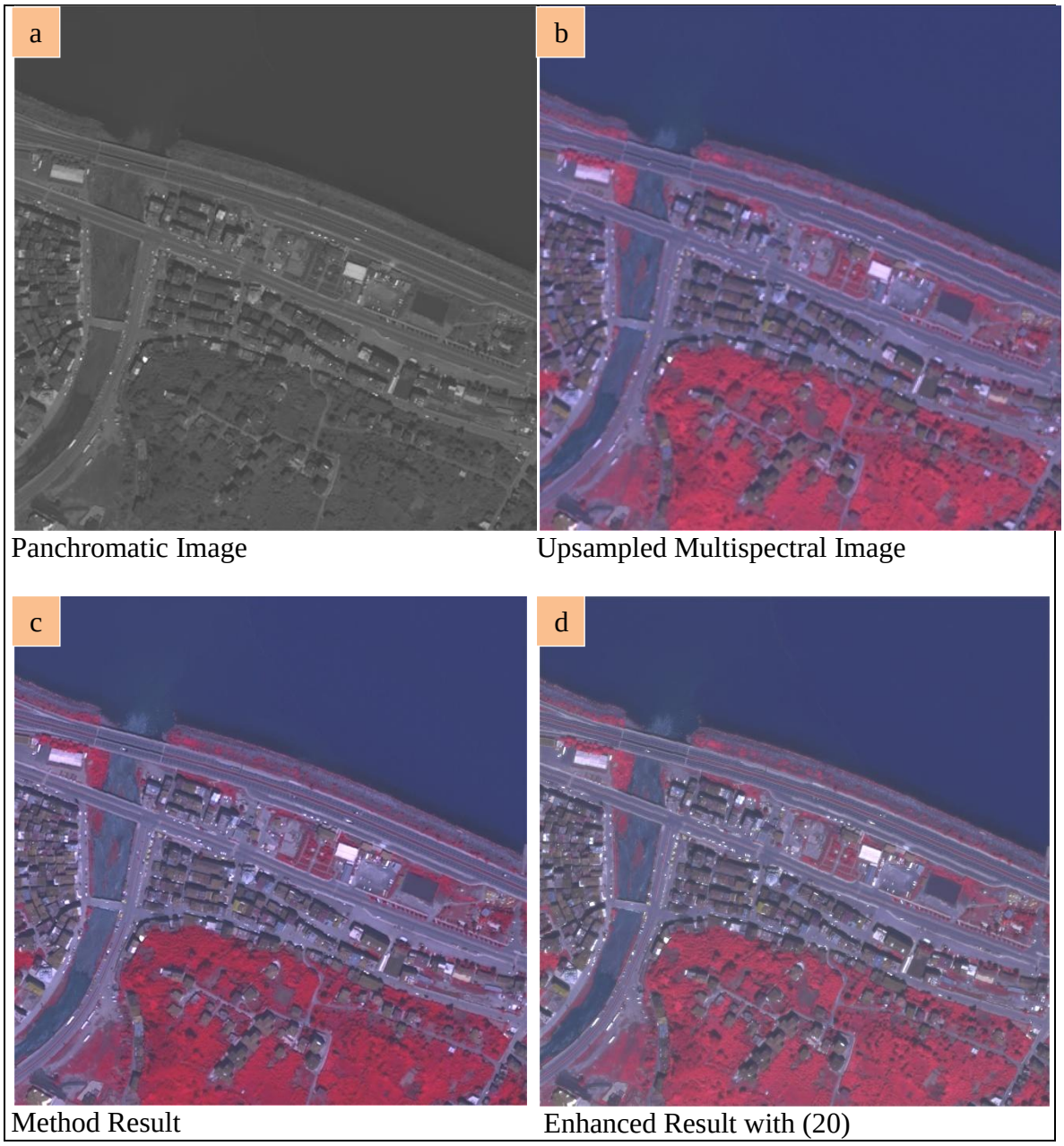

Figure 3.2. IHS images

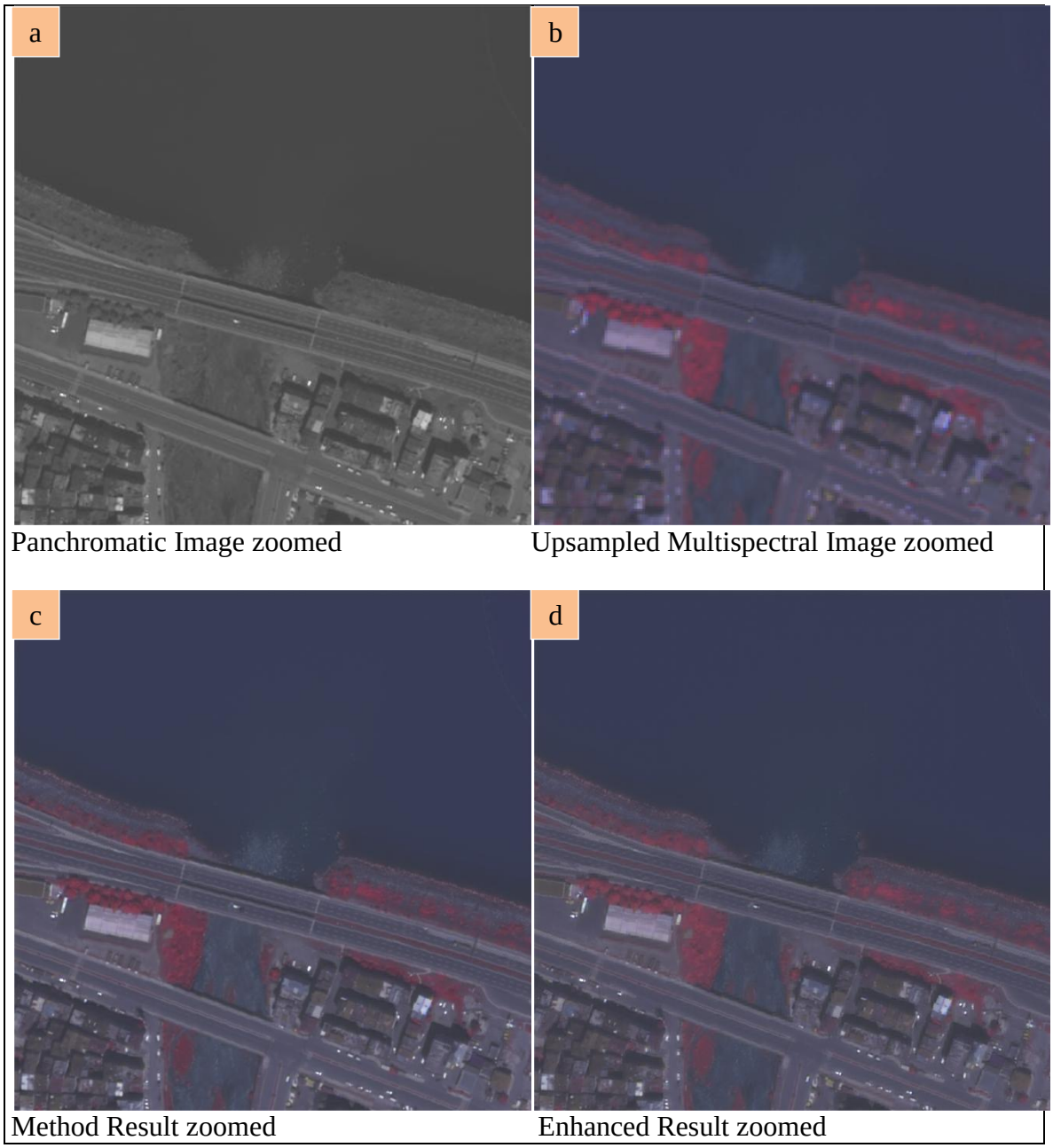

Figure 3.3. IHS images zoomed to the upper left quadrant

Table 3.6. IHS. Correlation statistics

	B1	**B2**	**B3**	**B4**	**B5**	**B6**	**B7**	**B8**
B1	1	0.9733	0.9399	0.8962	0.9027	0.4378	0.1729	0.0788
B2	0.9733	1	0.9685	0.8707	0.9162	0.4145	0.1718	0.063
B3	0.9399	0.9685	1	0.9119	0.9357	0.5206	0.2814	0.1804
B4	0.8962	0.8707	0.9119	1	0.9513	0.6966	0.4109	0.3517
B5	0.9027	0.9162	0.9357	0.9513	1	0.6599	0.418	0.3221
B6	0.4378	0.4145	0.5206	0.6966	0.6599	1	0.9023	0.8906
B7	0.1729	0.1718	0.2814	0.4109	0.418	0.9023	1	0.9571
B8	0.0788	0.063	0.1804	0.3517	0.3221	0.8906	0.9571	1
Sum	4.4016	4.378	4.7384	5.0893	5.1059	4.5223	3.3144	2.8437

Table 3.7. IHS. Fusion quality results

(19)	**IWSSIM**	**SSIM**	**CC**	**ERGAS**	**SID**
Method	0.9999	1.0000	0.0284	2.5376	0.0122
Final Enhancement	0.9430	0.9699	0.0249	0.2272	0.0000
(20)	**IWSSIM**	**SSIM**	**CC**	**ERGAS**	**SID**
Method	0.9999	1	0.0284	2.5376	0.0122
Final Enhancement	0.9707	0.984	0.1021	2.2848	0.0121

Table 3.8. IHS. Further radiometric statistics

(19)	**Diversity**	**Entropy**	**Th2.275%**	**MinMax**	**Contrast**
Method	10.9965	9.1469	[35,683]	[0,2047]	177.0921
Final Enhancement	10.9908	9.0792	[35,678]	[0,2047]	171.2027
(20)					
Method	10.9967	9.1469	[35,683]	[0,2047]	177.0921
Final Enhancement	10.9982	9.0446	[40,653]	[0,2047]	164.4923

3.3.2. PCA Method

The resulting images are shown in Figure 3.4. , and shown zoomed to the upper left quadrant in Figure 3.5. There is a big color distortion.

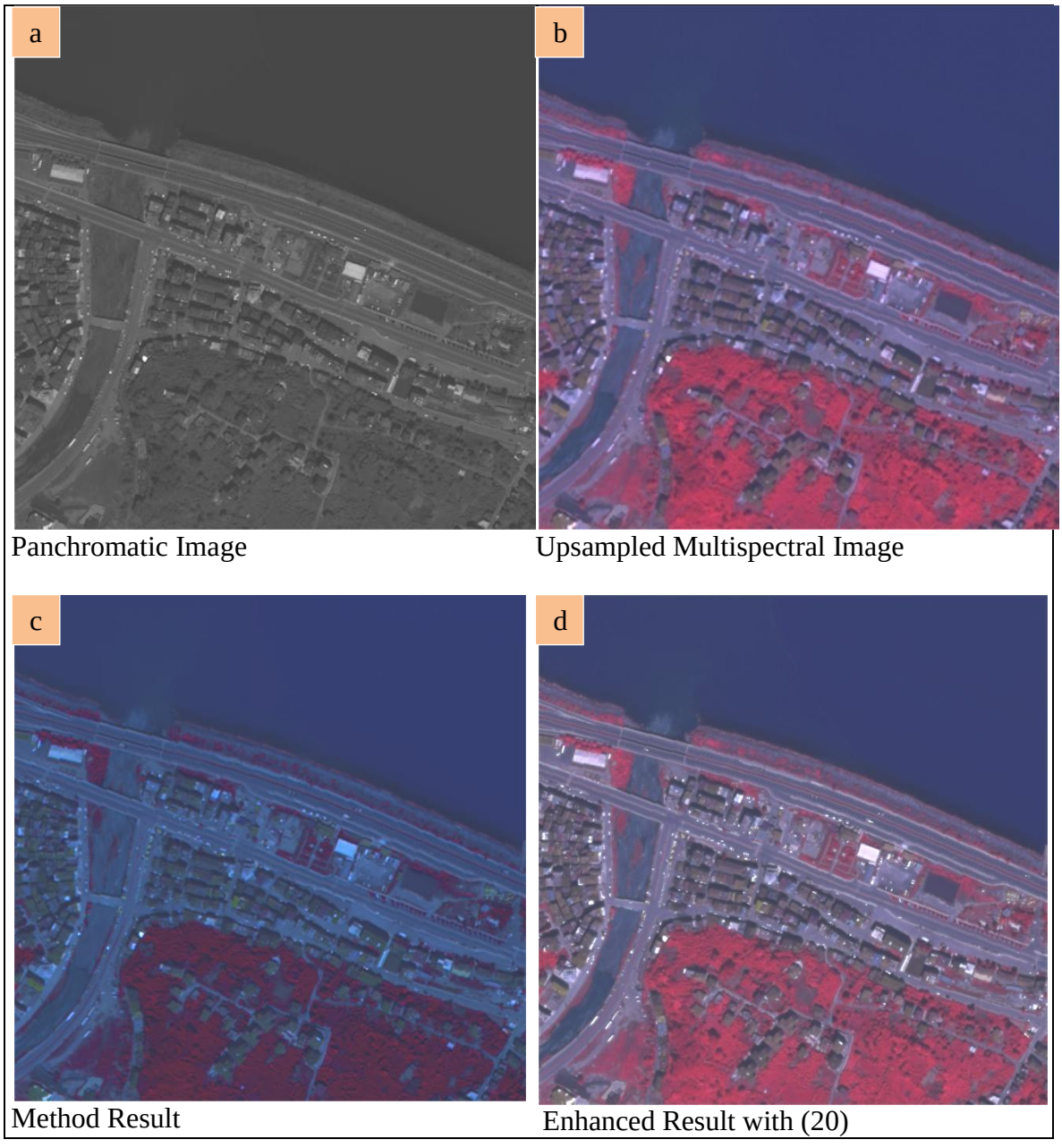

Figure 3.4. PCA images

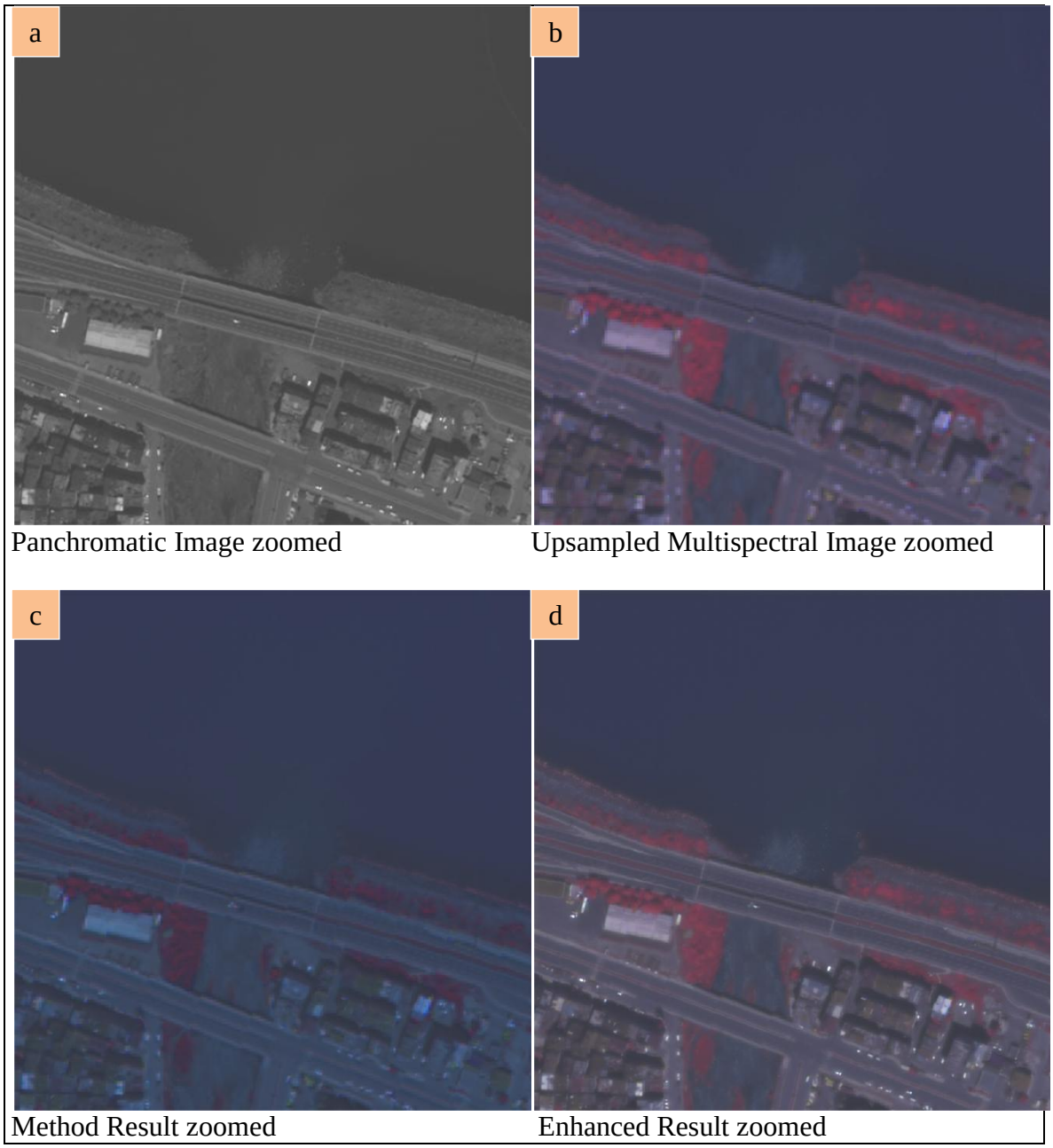

Figure 3.5. PCA images zoomed to the upper left quadrant

Table 3.9. PCA. Correlation statistics

	B1	**B2**	**B3**	**B4**	**B5**	**B6**	**B7**	**B8**
B1	1	0.932	0.9096	0.9309	0.8462	0.6832	0.1054	0.1191
B2	0.932	1	0.9751	0.8917	0.8944	0.653	0.0477	0.1164
B3	0.9096	0.9751	1	0.8886	0.8945	0.6643	0.0046	0.0952
B4	0.9309	0.8917	0.8886	1	0.9165	0.7964	0.0458	0.0532
B5	0.8462	0.8944	0.8945	0.9165	1	0.7954	0.1248	0.0367
B6	0.6832	0.653	0.6643	0.7964	0.7954	1	0.3431	0.355
B7	0.1054	0.0477	0.0046	0.0458	0.1248	0.3431	1	0.7075
B8	0.1191	0.1164	0.0952	0.0532	0.0367	0.355	0.7075	1
Sum	4.5264	4.5103	4.4319	4.5231	4.5085	4.2904	1.3789	1.4831

Table 3.10. PCA. Fusion quality results

(19)	**IWSSIM**	**SSIM**	**CC**	**ERGAS**	**SID**
Method	0.8043	0.8381	0.1722	9.3376	0.2871
Final Enhancement	0.9100	0.9633	0.0060	0.2816	0.0000
(20)	**IWSSIM**	**SSIM**	**CC**	**ERGAS**	**SID**
Method	0.8043	0.8381	0.1722	9.3376	0.2871
Final Enhancement	0.9593	0.9817	0.0957	2.3536	0.012

Table 3.11. PCA. Further radiometric statistics

(19)	**Diversity**	**Entropy**	**Th2.275%**	**MinMax**	**Contrast**
Method	10.4179	8.5060	[1,446]	[0,1587]	128.8692
Final Enhancement	10.9665	9.0153	[36,669]	[0,2047]	168.7463
(20)					
Method	10.4179	8.506	[1,446]	[0,1587]	128.8692
Final Enhancement	10.9936	9.0133	[40,647]	[0,2047]	162.3722

3.3.3. Haar Wavelet Method

The resulting images are shown in Figure 3.6. , and shown zoomed to the upper left quadrant in Figure 3.7.

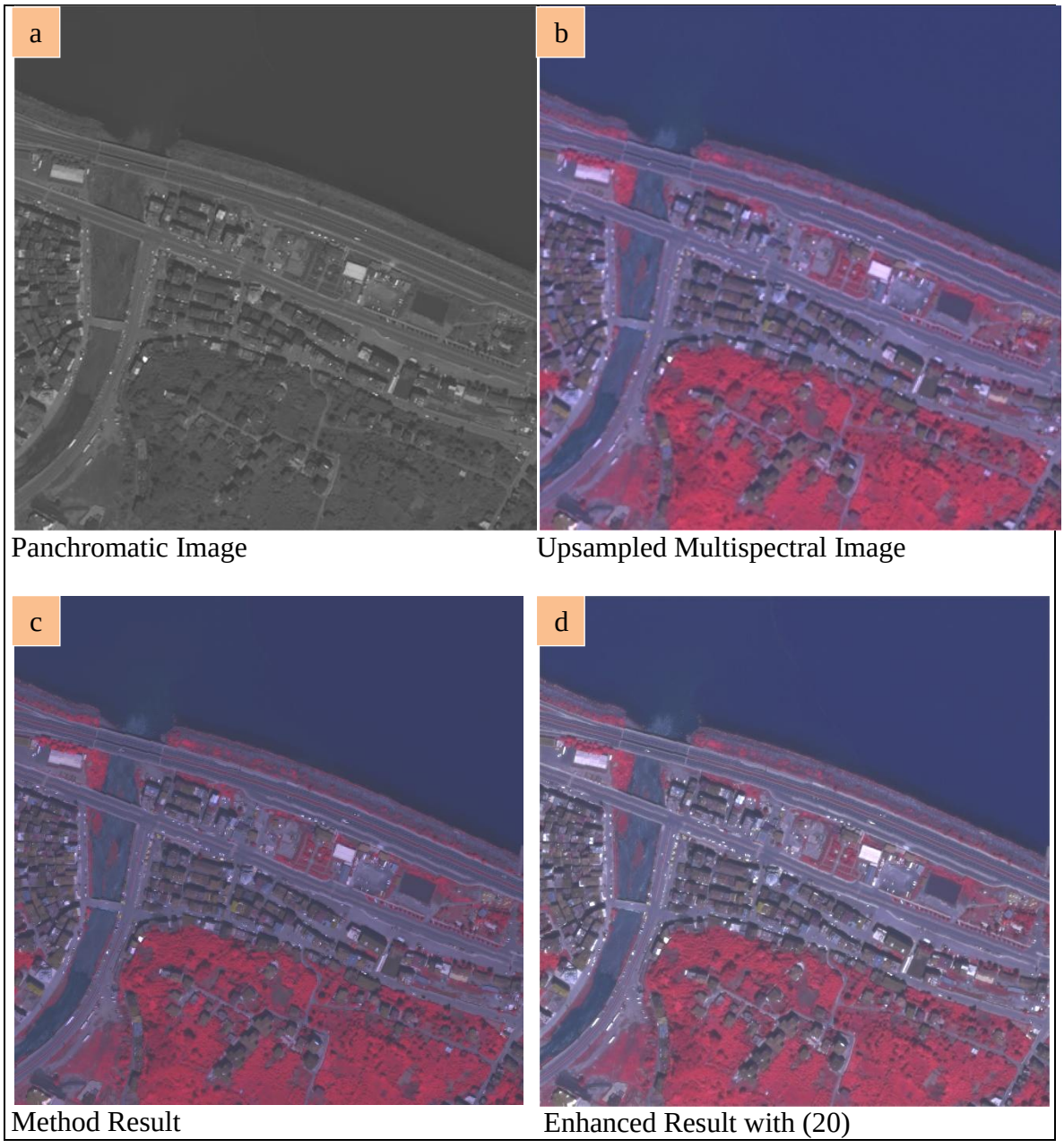

Figure 3.6. Haar wavelet images

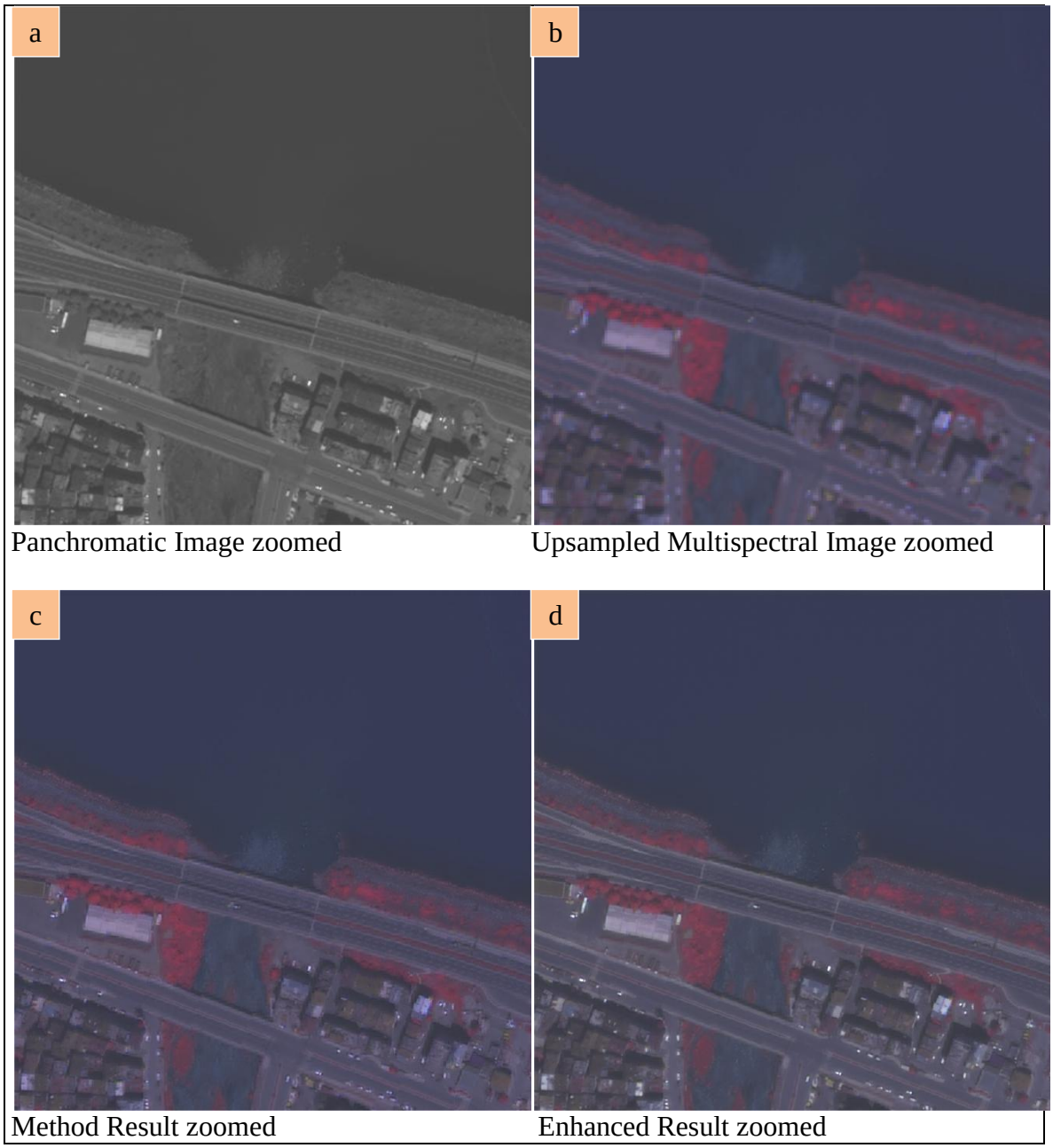

Figure 3.7. Haar wavelet images zoomed to the upper left quadrant

Table 3.12. Haar wavelet. Correlation statistics

	B1	**B2**	**B3**	**B4**	**B5**	**B6**	**B7**	**B8**
B1	1	0.9494	0.9023	0.8686	0.856	0.4425	0.1834	0.1552
B2	0.9494	1	0.9546	0.834	0.8808	0.4068	0.1735	0.1265
B3	0.9023	0.9546	1	0.8853	0.905	0.4973	0.2557	0.2133
B4	0.8686	0.834	0.8853	1	0.9366	0.677	0.3754	0.3722
B5	0.856	0.8808	0.905	0.9366	1	0.6662	0.4177	0.3781
B6	0.4425	0.4068	0.4973	0.677	0.6662	1	0.9016	0.9098
B7	0.1834	0.1735	0.2557	0.3754	0.4177	0.9016	1	0.9657
B8	0.1552	0.1265	0.2133	0.3722	0.3781	0.9098	0.9657	1
Sum	4.3574	4.3256	4.6135	4.9491	5.0404	4.5012	3.273	3.1208

Table 3.13. Haar. Fusion quality results

(19)	**IWSSIM**	**SSIM**	**CC**	**ERGAS**	**SID**
Method	0.9433	0.9696	0.0244	0.0672	0.0000
Spatial Enhancement	0.9444	0.9703	0.0270	0.2288	0.0000
(20)	**IWSSIM**	**SSIM**	**CC**	**ERGAS**	**SID**
Method	0.9433	0.9696	0.0244	0.0672	0
Spatial Enhancement	0.9706	0.9839	0.1019	2.2848	0.0121

Table 3.14. Haar. Further radiometric statistics

(19)	**Diversity**	**Entropy**	**Th2.275%**	**MinMax**	**Contrast**
Method	10.9687	9.0854	[35,678]	[0,2047]	171.2563
Spatial Enhancement	10.9901	9.0857	[35,679]	[0,2047]	171.5571
(20)					
Method	10.96854305	9.0854	[35,678]	[0,2047]	171.2563
Spatial Enhancement	10.99823414	9.0437	[40,653]	[0,2047]	164.4342

3.3.4. Brovey Method

The resulting images are shown in Figure 3.8. , and shown zoomed to the upper left quadrant in Figure 3.9. There is a big distortion in brightness levels and colors.

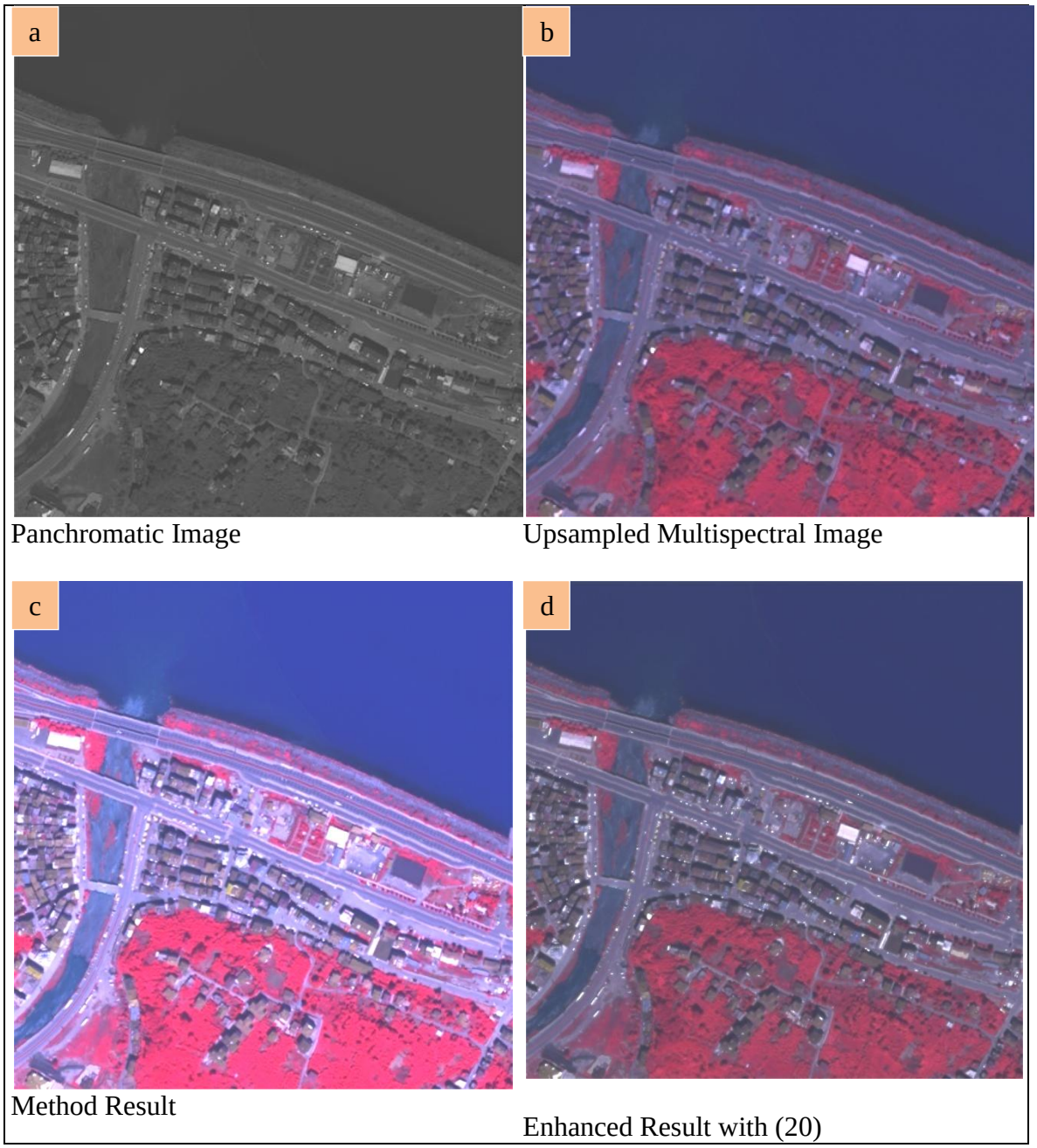

Figure 3.8. Brovey images

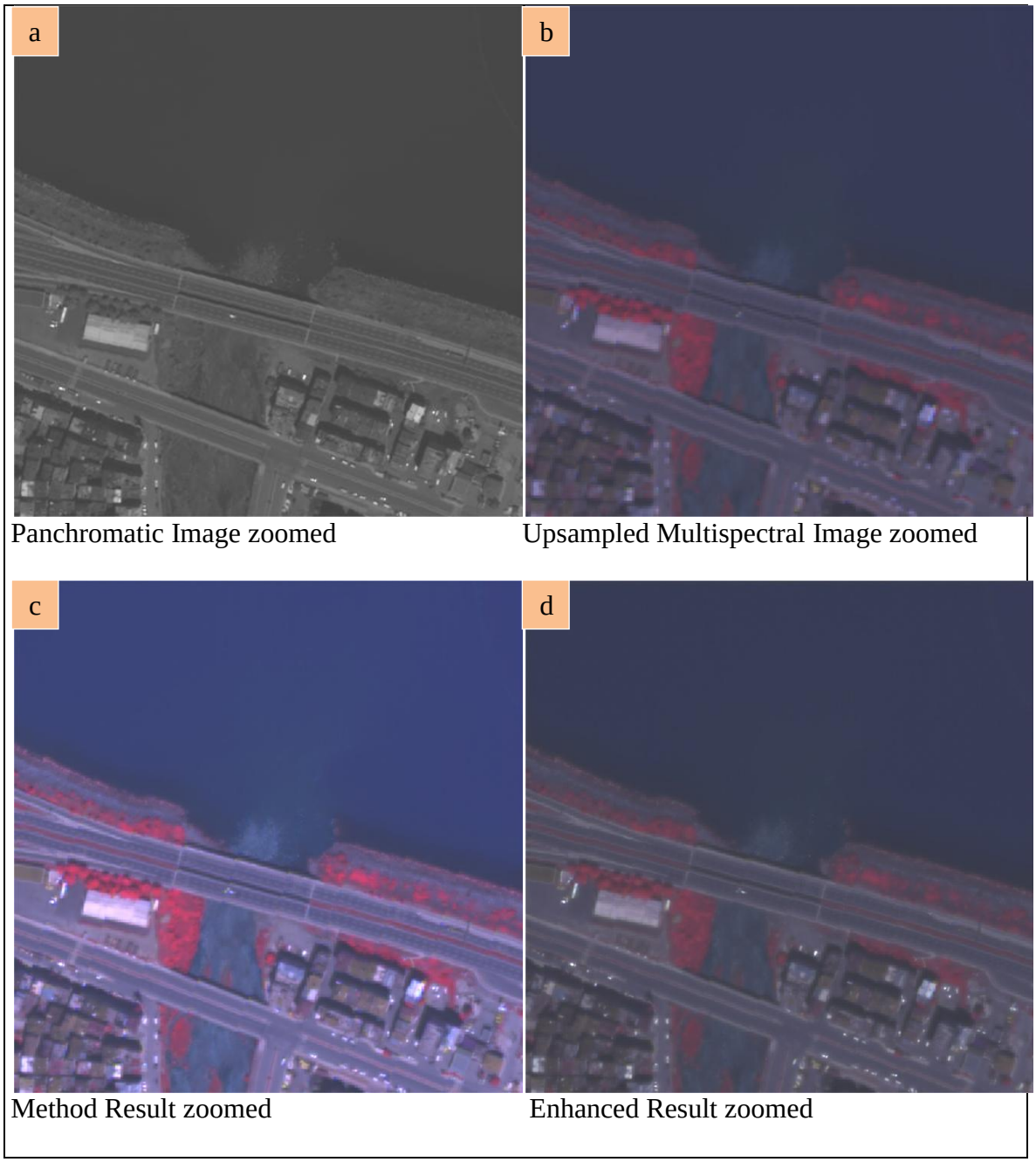

Figure 3.9. Brovey images zoomed to the upper left quadrant

The IWSSIM value got even worse during the spectral modification. The spectrally enhanced image fails the criteria of a spectral component.

Table 3.15. Brovey. Correlation statistics

	B1	**B2**	**B3**	**B4**	**B5**	**B6**	**B7**	**B8**
B1	1	0.9481	0.9179	0.8819	0.8262	0.4154	0.0968	0.0887
B2	0.9481	1	0.9729	0.8638	0.8678	0.4193	0.1315	0.1055
B3	0.9179	0.9729	1	0.8926	0.8995	0.5157	0.2483	0.217
B4	0.8819	0.8638	0.8926	1	0.946	0.7097	0.3998	0.4034
B5	0.8262	0.8678	0.8995	0.946	1	0.7097	0.4447	0.4177
B6	0.4154	0.4193	0.5157	0.7097	0.7097	1	0.8955	0.9045
B7	0.0968	0.1315	0.2483	0.3998	0.4447	0.8955	1	0.9646
B8	0.0887	0.1055	0.217	0.4034	0.4177	0.9045	0.9646	1
Sum	4.175	4.3089	4.6639	5.0972	5.1116	4.5698	3.1812	3.1014

Table 3.16. Brovey. Fusion quality results

(19)	**IWSSIM**	**SSIM**	**CC**	**ERGAS**	**SID**
Method	0.8713	0.7340	0.0189	18.9904	0.0001
Final Enhancement	0.8735	0.9575	0.0040	0.3104	0.0000
(20)	**IWSSIM**	**SSIM**	**CC**	**ERGAS**	**SID**
Method	0.8713	0.734	0.0189	18.9904	0.0001
Final Enhancement	0.9402	0.979	0.0917	0.3104	0.0121

Table 3.17. Brovey. Further radiometric statistics

(19)	**Diversity**	**Entropy**	**Th2.275%**	**MinMax**	**Contrast**
Method	10.9694	10.0038	[67,1017]	[29,2047]	235.3758
Spatial Enhancement	10.9204	8.9958	[36,665]	[15,2047]	167.9907
(20)					
Method	10.9693	10.0038	[63,1007]	[29,2047]	225.7722
Final Enhancement	10.9647	9.001	[40,643]	[31,2047]	161.3807

3.3.5. Covariance Based Method

The resulting images are shown in Figure 3.10. , and shown zoomed to the upper left quadrant in Figure 3.11.

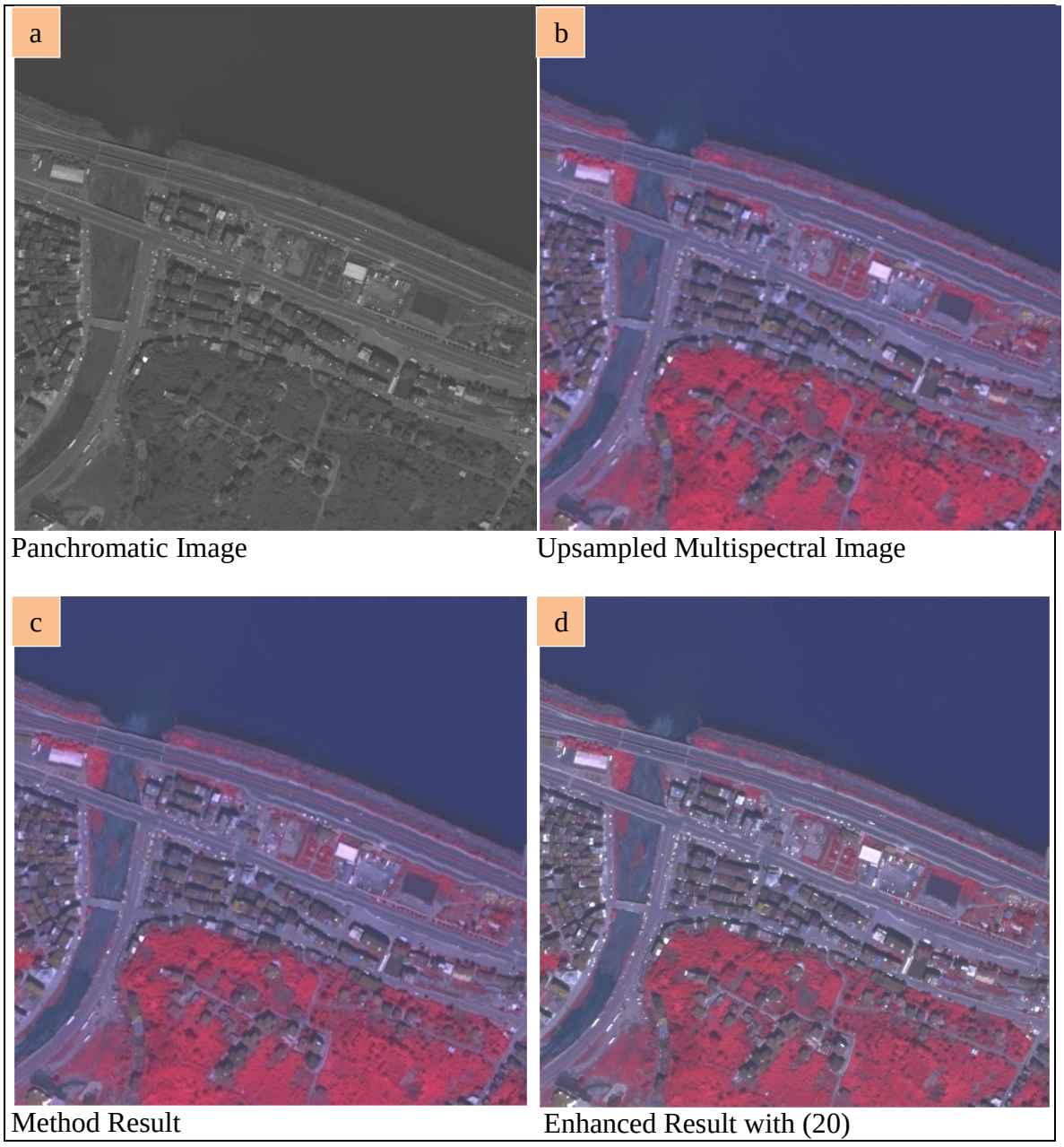

Figure 3.10. Covariance based method images.

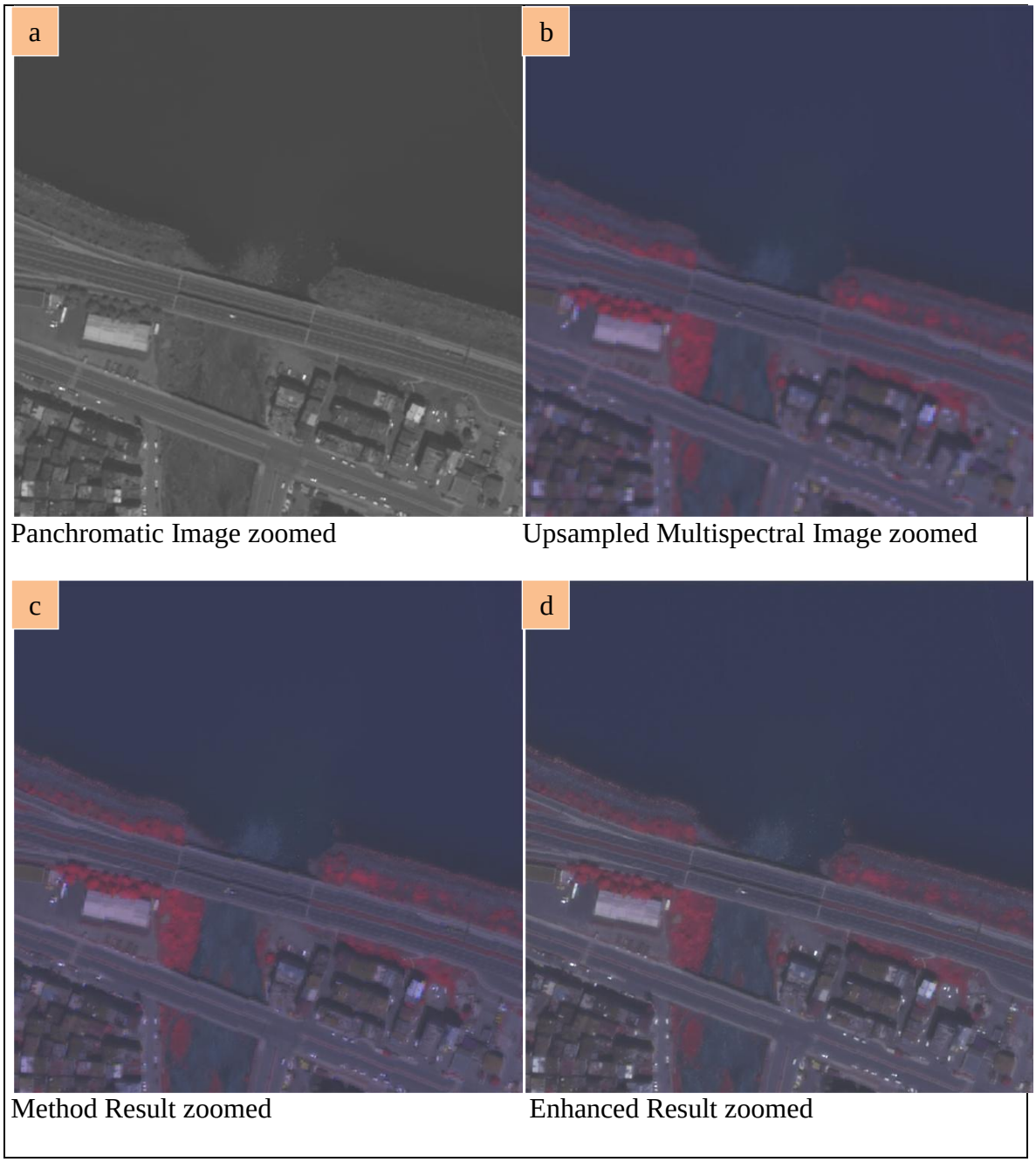

Figure 3.11. Covariance based method images zoomed to the upper left quadrant.

Table 3.18. Covariance based method. Correlation statistics

	B1	**B2**	**B3**	**B4**	**B5**	**B6**	**B7**	**B8**
B1	1	0.9332	0.9111	0.9057	0.844	0.4419	0.1287	0.1336
B2	0.9332	1	0.97	0.8614	0.8722	0.4003	0.1191	0.1019
B3	0.9111	0.97	1	0.8864	0.8979	0.4974	0.2364	0.2122
B4	0.9057	0.8614	0.8864	1	0.944	0.682	0.3724	0.3803
B5	0.844	0.8722	0.8979	0.944	1	0.6743	0.4044	0.3835
B6	0.4419	0.4003	0.4974	0.682	0.6743	1	0.901	0.911
B7	0.1287	0.1191	0.2364	0.3724	0.4044	0.901	1	0.9679
B8	0.1336	0.1019	0.2122	0.3803	0.3835	0.911	0.9679	1
Sum	4.2982	4.2581	4.6114	5.0322	5.0203	4.5079	3.1299	3.0904

Table 3.19. Covariance based method. Fusion quality results

(19)	**IWSSIM**	**SSIM**	**CC**	**ERGAS**	**SID**
Method	0.9367	0.9678	0.0144	0.0480	0.0000
Spatial Enhancement	0.9382	0.9687	0.0177	0.2448	0.0000
(20)	**IWSSIM**	**SSIM**	**CC**	**ERGAS**	**SID**
Method	0.9367	0.9678	0.0144	0.0480	0
Spatial Enhancement	0.9687	0.9834	0.1009	2.3168	0.0122

Table 3.20. Covariance based method. Further radiometric statistics

(19)	**Diversity**	**Entropy**	**Th2.275%**	**MinMax**	**Contrast**
Method	10.9744	9.0578	[35,676]	[0,2047]	170.4959
Spatial Enhancement	10.9858	9.0585	[36,677]	[0,2047]	170.7771
(20)					
Method	10.9744	9.0578	[35,676]	[0,2047]	170.4959
Spatial Enhancement	10.9952	9.0338	[40,652]	[0,2047]	163.7116

3.3.6. Least Squares Based Method

The resulting images are shown in Figure 3.12. , and shown zoomed to the upper left quadrant in Figure 3.13.

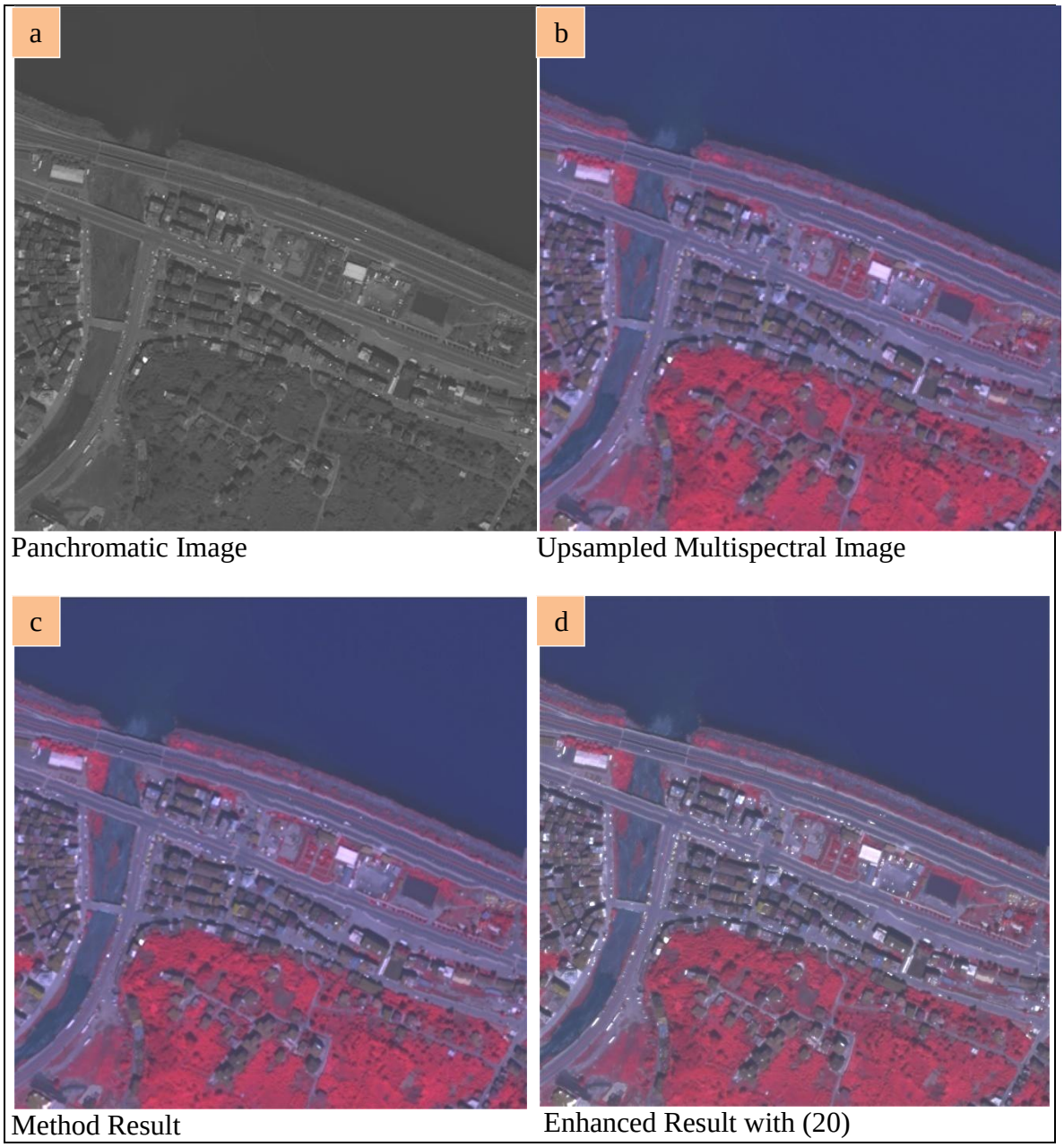

Figure 3.12. Least squares method images.

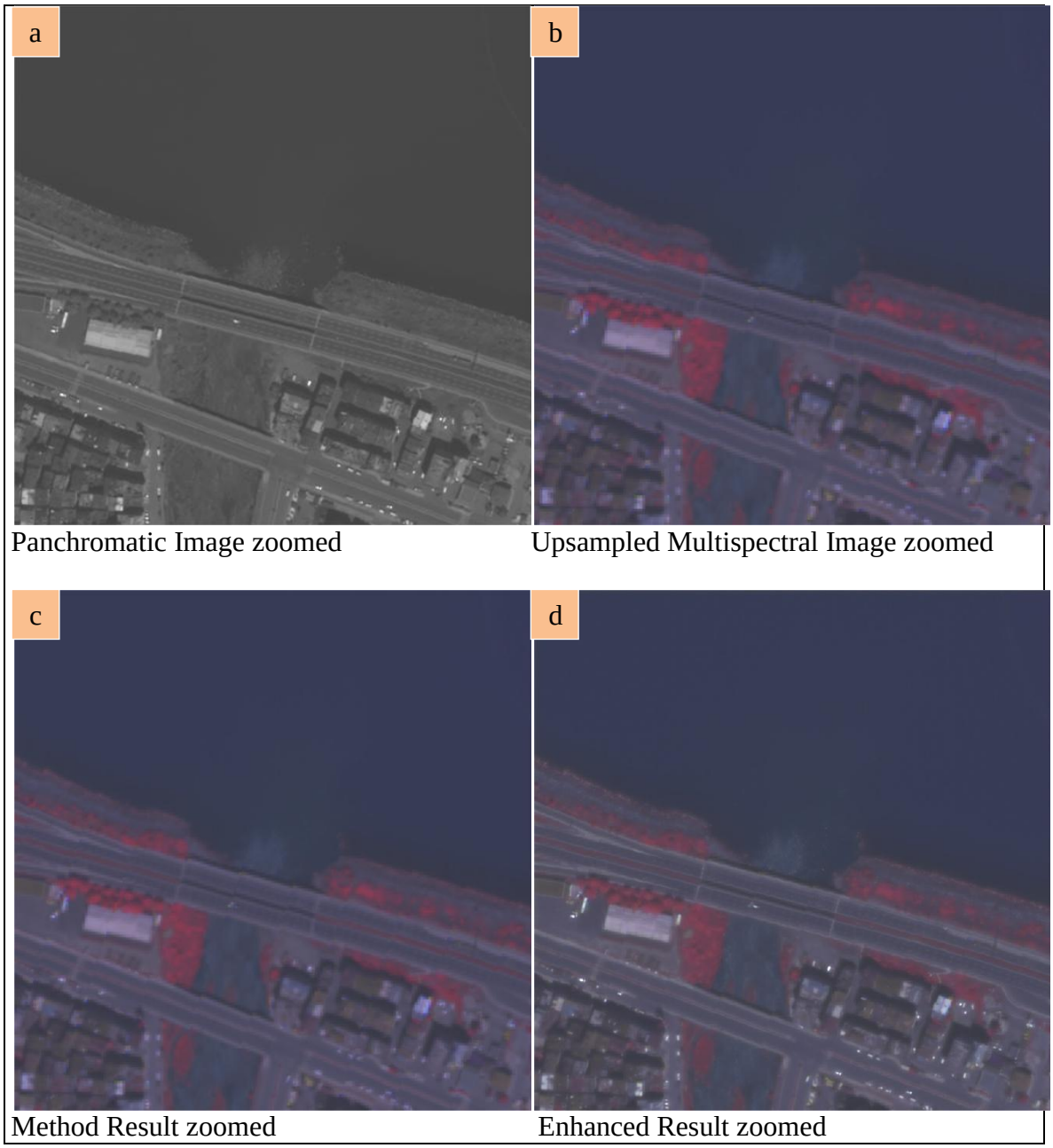

Figure 3.13. Least squares method images zoomed to the upper left quadrant.

Table 3.21. Least squares based method. Correlation statistics

	B1	**B2**	**B3**	**B4**	**B5**	**B6**	**B7**	**B8**
B1	1	0.9128	0.9045	0.8988	0.8291	0.4144	0.0959	0.1021
B2	0.9128	1	0.9624	0.8507	0.8672	0.3703	0.0903	0.0691
B3	0.9045	0.9624	1	0.8808	0.8919	0.4718	0.2075	0.1816
B4	0.8988	0.8507	0.8808	1	0.9395	0.6639	0.3464	0.354
B5	0.8291	0.8672	0.8919	0.9395	1	0.654	0.3796	0.3559
B6	0.4144	0.3703	0.4718	0.6639	0.654	1	0.898	0.9086
B7	0.0959	0.0903	0.2075	0.3464	0.3796	0.898	1	0.9665
B8	0.1021	0.0691	0.1816	0.354	0.3559	0.9086	0.9665	1
Sum	4.1576	4.1228	4.5005	4.9341	4.9172	4.381	2.9842	2.9378

Table 3.22. Least squares based method. Fusion quality results

(19)	**IWSSIM**	**SSIM**	**CC**	**ERGAS**	**SID**
Method	0.8864	0.9584	0.0029	0.0048	0.0000
Spatial Enhancement	0.8902	0.9601	0.0050	0.2848	0.0000
(20)	**IWSSIM**	**SSIM**	**CC**	**ERGAS**	**SID**
Method	0.8864	0.9584	0.0029	0.0048	0
Spatial Enhancement	0.9481	0.98	0.0918	2.3600	0.012

Table 3.23. Least squares based method. Further radiometric statistics

(19)	**Diversity**	**Entropy**	**Th2.275%**	**MinMax**	**Contrast**
Method	10.4988	9.1415	[89,676]	[3,1809]	150.2751
Spatial Enhancement	10.7432	9.1195	[102,687]	[36,2047]	153.4124
(20)					
Method	10.4988	9.1415	[89,676]	[3,1809]	150.2751
Spatial Enhancement	10.9678	9.0037	[40,643]	[31,2047]	161.6324

3.3.7. Changing Flexibility Function Parameters

First, the covariance based method is applied to the multispectral image 2. For flexibility demonstration, the flexibility series function, the parameter r is changed.

Table 3.24. Flexibility function and parameter change. Fusion quality results

(19)	**IWSSIM**	**SSIM**	**CC**	**ERGAS**	**SID**
r=1/10	0.927	0.9227	0.0161	0.4032	0
r=4/5	0.9288	0.9243	0.0185	0.6704	0
(20)	**IWSSIM**	**SSIM**	**CC**	**ERGAS**	**SID**
r=1/10	0.9856	0.9842	0.1466	6.1472	0.0105
r=4/5	0.931	0.9264	0.0217	0.8624	0.0001

When r is close to 1, the fusion is spectrally better, and when r is close to 0, the fusion is spatially better. With function series in (20), the covariance based method is enhanced better spatially.

The function series in (19) turned out to be less sensitive in a change in the flexibility parameter.

4. DISCUSSION AND CONCLUSION

The primary objective of this research was to devise flexible and competitive methods for image fusion. Flexibility will be satisfied with the help spatially well fused images, but first the base image, the spectrally well fused image, needs to perform well.

The least squares based method turned out to be barely an underachiever with one iteration. More iterations should improve the results. Among the already existing techniques, PCA performed poorly.

The Brovey fused image is very sharp, which may make it visually appealing, but undesirable in many situations. IWSSIM values indicate a rather good spatial performance, but not strictly better than it is for the remaining techniques. Its ERGAS value is well over 3, indicating bad spectral quality. Scaling may improve the results.

The remaining techniques IHS, wavelet, and the covariance based technique performed at similar levels. IHS is ahead in terms of IWSSIM and SSIM values. The SSIM and IWSSIM values have risen to the levels above 0.9, yet the spectral quality has not deteriorated much, in general. The band correlations have generally increased, indicating some detoriation regarding the spectral content transfer quality. There was an artificial radiometric enhancement.

Correlation statistics of the fused images are often bigger than the correlation statistic of the multispectral image, indicating a loss in spectral information.

The covariance based technique is a competitive technique producing spectrally well fused images. The other proposed technique, least squares based technique, produced satisfactory results, worse than the covariance based technique.

SID testing was not effective.

A key finding is that covariance based method turned out to be the one that performed best in 3.1. The original multispectral image was downsampled along with the panchromatic image, creating a hypothetical setting for fusion. When those downsampled images were used, the one that turned out to have recovered most data from the original multispectral image is the covariance based technique, for all input image pairs.

The flexibility parameters changed the result. Statistics indicate that flexibility function series (20) gives better results than flexibility function series (19) for the same parameter, spatially. A better flexibility function series can improve the results even

further. From the graphics of the functions, one may be able to find a relation between flexibility parameters that give similar results. The functions (20) get more quickly closer to the limits. (19) can be redefined to decrease this difference. One choice is some convex combination.

Furthermore, the final fusion process enhanced the results, but not at desired levels. The statistics improved greatly for the underachievers, PCA and Brovey techniques. There was a spatial downgrade for IHS, according to the spatial statistics.

Following the secondary objective, the theoretical framework is intentionally set up in a way open to improvements.

5. REFERENCES

Aiazzi, B., Alparone, L., Baronti, S., Garzelli, A., Nencini, F. and Selva, M. 2004. Spectral Information Extraction by Means of Ms+ Pan Fusion, Proceedings of ESA-EUSC, 20.21.

Amolins, K., Zhang, Y. and Dare, P. 2007. Wavelet Based Image Fusion Techniques—an Introduction, Review and Comparison, ISPRS Journal of Photogrammetry and Remote Sensing, 62, 4, 249-263.

Bierstedt, K.D. and Bonet, J. 2003. Some Aspects of the Modern Theory of Fréchet Spaces, Revista de la Real Academia de Ciencias Exactas, Físicas y Naturales. Serie A: Matemáticas (RACSAM), 97, 2, 159.

Book, G. 1993. IUPAC Quantities, Units and Symbols in Physical Chemistry, 2nd, Blackwell Scientific Publications.

Chang, C.I. 1999. Spectral Information Divergence for Hyperspectral Image Analysis, Geoscience and Remote Sensing Symposium, 1999. IGARSS'99 Proceedings. IEEE 1999 International, 1, 509-511.

Chavez, P. 1989. Extracting Spectral Contrast in Landsat Thematic Mapper Image Data Using Selective Principal Component Analysis, Photogrammetric Engineering and Remote Sensing, 55, 339-348.

Chen, C. 2012. Signal and Image Processing for Remote Sensing, CRC press.

Chibani, Y. and Houacine, A. 2002. The Joint Use of Ihs Transform and Redundant Wavelet Decomposition for Fusing Multispectral and Panchromatic Images, International Journal of Remote Sensing, 23, 18, 3821-3833.

Choi, M., Kim, H., Cho, N. and Kim, H. 2006. An Improved Intensity-Hue-Saturation Method for Ikonos Image Fusion, International Journal of Remote Sensing,

Chui, C.K. 1992. An Introduction to Wavelets, 1, Academic Pr.

Cliche, G., Bonn, F. and Teillet, P. 1985. Integration of the Spot Panchromatic Channel into Its Multispectral Mode for Image Sharpness Enhancement, Photogrammetric Engineering and Remote Sensing, 51, 311-316.

Cornet, Y., De Béthune, S., Binard, M., Muller, F., Legros, G. and Nadasdi, I. 2001. Rs Data Fusion by Local Mean and Variance Matching Algorithms: Their Respective Efficiency in a Complex Urban Context, Remote Sensing and Data Fusion over Urban Areas, IEEE/ISPRS Joint Workshop 2001, 105-111.

Dutka, J. 1984. The Early History of the Hypergeometric Function, Archive for History of Exact Sciences, 31, 1, 15-34.

Elachi, C. and Van Zyl, J.J. 2006. Introduction to the Physics and Techniques of Remote Sensing, 28, Wiley-Interscience.

Farge, M. and Schneider, K. 2006. Wavelets: Application to Turbulence, Encyclopedia of Mathematical Physics, 408-420.

González-Audícana, M., Otazu., X., Fors, O., and Alvarez-Mozos, J. 2006. A Low Computational-Cost Method to Fuse Ikonos Images Using the Spectral Response Function of Its Sensors, Geoscience and Remote Sensing, IEEE Transactions on, 44, 6, 1683-1691.

González-Audícana, M., Saleta, JL., Catalán, R.G. and García, R. 2004. Fusion of Multispectral and Panchromatic Images Using Improved Ihs and Pca Mergers Based on Wavelet Decomposition, Geoscience and Remote Sensing, IEEE Transactions on, 42, 6, 1291-1299.

Gonzalez-Audicana, M., Otazu, X., Fors, O. and Seco, A. 2005. Comparison between Mallat's and the 'À Trous' Discrete Wavelet Transform Based Algorithms for the Fusion of Multispectral and Panchromatic Images, International Journal of Remote Sensing, 26, 3, 595-614.

Gonzalez, R. and Woods, R. 2008. Digital Image Processing., Prentice-Hall Inc.
.
Goshtasby, A.A. 2005. 2-D and 3-D Image Registration: For Medical, Remote Sensing, and Industrial Applications, Wiley-Interscience.

Gungor, O. 2008. Multi Sensor Multi Resolution Image Fusion, PhD, Purdue University.

Hamza, A.B., He, Y., Krim, H. and Willsky, A. 2005. A Multiscale Approach to Pixel-Level Image Fusion, Integrated Computer Aided Engineering, 12, 2, 135-146.

Harrison, B.A., Jupp, D.L.B. and Scientific, C. 1990. Introduction to Image Processing, CSIRO Australia, Division of Water Resources.

Hill, J., Diemer, C., Stöver, O. and Udelhoven, T. 1999. A Local Correlation Approach for the Fusion of Remote Sensing Data with Different Spatial Resolutions in Forestry Applications, International Archives of Photogrammetry and Remote Sensing, 32, 7, 4-3.

Hossny, M., Nahavandi, S. and Crieghton, D. 2008. Feature-Based Image Fusion Quality Metrics, Intelligent Robotics and Applications, 469-478.

Jinghui, Y., Jixian, Z., Haitao, L., Yushan, S. and Pengxian, P. 2010. Pixel Level Fusion Methods for Remote Sensing Images: A Current,

Konecny, G. 2003. Geoinformation: Remote Sensing, Photogrammetry and Geographic Information Systems, Taylor & Francis.

Kuczma, M. 2008. An Introduction to the Theory of Functional Equations and Inequalities: Cauchy's Equation and Jensen's Inequality, Birkhäuser Basel.

Lancaster, J. 1968. Geographers and Remote Sensing, Journal of Geography, 67, 5, 301-310.

Li, H., Manjunath, B. and Mitra, S.K. 1995. Multisensor Image Fusion Using the Wavelet Transform, Graphical models and image processing, 57, 3, 235-245.

Liang, S. 2004. Quantitative Remote Sensing of Land Surfaces, John Wiley & Sons, Inc.

Madden, C.K. 2011. Contributions to Remote Sensing of Shallow Water Depth with the Worldview-2 Yellow Band, MS, Naval Postgraduate School.

Mahyari, A.G. and Yazdi, M. 2011. Remote Sensing Image Fusion Using Gramian as a Rule of Fusion, International Journal of Electronics, 98, 3, 279-287.

Mihov, S.G. and Zapryanov, G.S. 2005. Interpolation Algorithms for Image Scaling, Proceedings of the Fourteenth International Scientific and Applied Science Conference-Electronics' 2005, 162-167.

Nayak, S. and Zlatanova, S. 2008. Remote Sensing and Gis Technologies for Monitoring and Prediction of Disasters, Springer.

Neitz, J., Carroll, J. and Neitz, M. 2001. Almost Reason Enough for Having Eyes, Optics & Photonics News, 27,

Nikolakopoulos, K.G. 2008. Comparison of Nine Fusion Techniques for Very High Resolution Data, Photogrammetric Engineering and Remote Sensing, 74, 5, 647.

Padwick, C., Deskevich, M., Pacifici, F. and Smallwood, S. 2010. Worldview-2 Pan-Sharpening, American Society for Photogrammetry and Remote Sensing,

Peli, E. 1990. Contrast in Complex Images, JOSA A, 7, 10, 2032-2040.

Pohl, C. and Van Genderen, J. 1998. Review Article Multisensor Image Fusion in Remote Sensing: Concepts, Methods and Applications, International Journal of Remote Sensing, 19, 5, 823-854.

Pradhan, P.S., King, R.L., Younan, N.H. and Holcomb, D.W. 2006. Estimation of the Number of Decomposition Levels for a Wavelet-Based Multiresolution Multisensor Image Fusion, Geoscience and Remote Sensing, IEEE Transactions on, 44, 12, 3674-3686.

Pratt, W.K. 2001. Digital Image Processing: Piks Inside, John Wiley & Sons, Inc.

Rahmani, S., Strait, M., Merkurjev, D., Moeller, M. and Wittman, T. 2010. An Adaptive Ihs Pan-Sharpening Method, Geoscience and Remote Sensing Letters, IEEE, 7, 4, 746-750.

Rees, W.G. 2001. Physical Principles of Remote Sensing, 1, Cambridge University Press.

Schott, J.R. 2007. Remote Sensing: The Image Chain Approach, Oxford University Press, USA.

Schowengerdt, R.A. 2006. Remote Sensing: Models and Methods for Image Processing, Academic press.

Švab, A. and Oštir, K. 2006. High-Resolution Image Fusion: Methods to Preserve Spectral and Spatial Resolution, Photogrammetric Engineering & Remote Sensing, 72, 5, 565-572.

Tu, T.M., Huang, P.S., Hung, C.L. and Chang, C.P. 2004. A Fast Intensity-Hue-Saturation Fusion Technique with Spectral Adjustment for Ikonos Imagery, Geoscience and Remote Sensing Letters, IEEE, 1, 4, 309-312.

URL-1, http://www.nrcan.gc.ca/sites/www.nrcan.gc.ca.earth-sciences/files/pdf/resource/tutor/fundam/pdf/fundamentals_e.pdf. 09 Kasım 2012.

URL-2, http://en.wikipedia.org/wiki/Image_resolution. 09 Kasım 2012.

URL-3, http://www.grasdk.com/~/media/Microsite_GRAS/Files/WorldView2.ashx. 09 Kasım 2012.

URL-4, http://www.math.umn.edu/~garrett/m/fun/Notes/seminorms.pdf. 09 Kasım 2012.

URL-5, http://planetmath.org/SemiInnerProduct.html. 09 Kasım 2012.

URL-6, http://tr.wikipedia.org/wiki/Trabzon_(il). 09 Kasım 2012.

URL-7, http://www.karalahana.com/karadeniz/surmene-cografya.htm. 11 Kasım 2012.

Wald, L. 2000. Quality of High Resolution Synthesised Images: Is There a Simple Criterion?, Proceedings, 99-103.

Wald, L, Ranchin, T and Mangolini, M. 1997. Fusion of Satellite Images of Different Spatial Resolutions: Assessing the Quality of Resulting Images, Photogrammetric Engineering & Remote Sensing, 63, 6, 691-699.

Wang, P. and Liu, B. 2008. A Novel Image Fusion Metric Based on Multi-Scale Analysis, ICSP 2008, 965-968.

Wang, Z., Bovik, A.C., Sheikh, HR and Simoncelli, EP. 2004. Image Quality Assessment: From Error Visibility to Structural Similarity, Image Processing, IEEE Transactions on, 13, 4, 600-612.

Wang, Z. and Li, Q. 2011. Information Content Weighting for Perceptual Image Quality Assessment, Image Processing, IEEE Transactions on, 20, 5, 1185-1198.

Wang, Z. and Shang, X. 2006. Spatial Pooling Strategies for Perceptual Image Quality Assessment, Image Processing, 2006 IEEE International Conference on, 2945-2948.

Yang, S., Wang, M. and Jiao, L. 2012. Fusion of Multispectral and Panchromatic Images Based on Support Value Transform and Adaptive Principal Component Analysis, Information Fusion, 13, 3, 177-184.

Yıldırım, D. and Güngör, O. 2012. Ikonos Uydu Görüntüleri ile Yeni Bir Görüntü Kaynaştırma Yöntemi, Jeodezi ve Jeoinformasyon Dergisi, 1,

Zhang, J. 2010. Multi-Source Remote Sensing Data Fusion: Status and Trends, International Journal of Image and Data Fusion, 1, 1, 5-24.

Zhang, Y. 2002. Problems in the Fusion of Commercial High-Resolution Satelitte as Well as Landsat 7 Images and Initial Solutions, International Archives of Photogrammetry Remote Sensing and Spatial Information Sciences, 34, 4, 587-592.

Zhang, Y. 2004. Understanding Image Fusion, Photogrammetric Engineering and Remote Sensing, 70, 6, 657-661.

Zhang, Y. 2008. Methods for Image Fusion Quality Assessment-a Review, Comparison and Analysis, The International Archives of the Photogrammetry, Remote Sensing and Spatial Information Sciences, 37, 1101-1109.

Zhang, Y. and Hong, G. 2005. An Ihs and Wavelet Integrated Approach to Improve Pan-Sharpening Visual Quality of Natural Colour Ikonos and Quickbird Images, Information Fusion, 6, 3, 225-234.

Zhao, S., Xue-Zhi, F., Kang, G. and Ramadan, E. 2002. Multi-Source Remote Sensing Image Fusion Based on Support Vector Machine, Chinese Geographical Science, 12, 3, 244-248.

Zhou, J., Civco, D. and Silander, J. 1998. A Wavelet Transform Method to Merge Landsat Tm and Spot Panchromatic Data, International Journal of Remote Sensing, 19, 4, 743-757.

ÖZGEÇMİŞ

1978 yılında İstanbul'da doğdu. Orta ve lise öğrenimini İstanbul Lisesi'nde tamamladı. 1997 yılında, Bilkent Üniversitesi burslu Matematik Bölümü'nde olarak lisans öğrenimine başladı. 2000–2001 eğitim öğretim yılında bölümü üçüncülükle tamamladı. 2001 yılında doktora öğrenimine Purdue Üniversitesi'nde (ABD) Matematik bölümünde başladı. 2001-2008 yılları arasında aynı bölümde "lisansüstü araştırma görevlisi" olarak çalıştı; bölüm bünyesinde, çeşitli seviyelerde Calculus ve Cebir dersleri verdi. 2008 ve 2009 yıllarında yurt dışı eğitim danışmanlığı firmalarında danışmanlık görevi yaptı. 2009 yılında KTÜ Fen Bilimleri Enstitüsü Harita Mühendisliği Uzaktan Algılama anabilim dalında yüksek lisans eğitimine başladı. 2009 yılında KTÜ Mühendislik Fakültesi'nde Araştırma Görevlisi olarak çalışmaya başladı. Halen bu görevine devam etmekte olup çok iyi derecede İngilizce ve Almanca bilmektedir.